IEEE Access
Multidisciplinary | Rapid Review | Open Access Journal

Received 2 December 2023, accepted 12 December 2023, date of publication 18 December 2023,
date of current version 26 December 2023.

Digital Object Identifier 10.1109/ACCESS.2023.3344162

APPLIED RESEARCH

A Combined Framework Based on Feature Selection and Multivariate Mixed-Frequency for Crude Oil Prices Point and Interval Forecasting

JUN LONG[1], LUE LI[2,3], AND ZEJUN LI[1]

[1]School of Mathematics and Information Science, Guangxi University, Nanning 530003, China
[2]School of Big Data and Artificial Intelligence, Guangxi University of Finance and Economics, Nanning 530003, China
[3]Guangxi Key Laboratory of Big Data in Finance and Economics, Guangxi University of Finance and Economics, Nanning 530003, China

Corresponding author: Lue Li (lueli126@126.com)

This work was supported in part by the Guangxi Science and Technology Project under Grant GuikeAD21220082, in part by the Guangxi Key Laboratory of Big Data in Finance and Economics under Grant FED2202, and in part by the Guangxi First-Class Discipline Statistics Construction Project under Grant 2022SXYB08 and Grant TJYLXKDSJ2022A02.

ABSTRACT Effective crude oil price forecasting is essential for energy supply stabilization, investment decisions, policy formulation, and economic impact assessment. However, previous studies of crude oil futures price forecasting either consider only a single variable without adequately accounting for the influence of various factors on crude oil prices, or they consider only the same frequency of influences and ignore the importance of mixed frequencies, resulting in forecasts that do not achieve the desired results. To overcome these problems, this paper proposes a new multivariate combinatorial mixed frequency forecasting system to predict the weekly closing price of crude oil futures. The system is divided into four modules: Data denoising, Feature selection, Combined forecasting, and Performance evaluation module. To obtain smooth data, ICEEMDAN is used to denoise the original data. Furthermore, to select appropriate variables and reduce model redundancy, recursive feature elimination is used to select appropriate variables with low frequency. Considering the importance of mixed-frequency data, the mutual information method was used to select appropriate high-frequency variables for modeling the crude oil price forecast model. To overcome the shortcomings of Back Propagation Neural Network, Gate Recurrent Unit, and Radial Basis Function Neural Network models, integrate their advantages, and obtain accurate and stable prediction results, a combined forecasting mechanism based on a Multi-Objective Sparrow Search algorithm was developed to obtain both point and interval forecasting results, and finally, two data sets were selected for empirical analysis. The results show that the mean absolute percentage errors of the point forecast of this model are 1.96% and 1.84%, respectively, about 31% and 15% higher than those of the competing models (mean absolute percentage errors 2.57% and 2.13%, respectively). For interval forecasting, the accumulated width deviation is 0.0037 and 0.002, respectively, about 35% and 25% higher than those of the competing models (accumulated width deviation 0.005 and 0.0025, respectively). Thus, the proposed forecasting framework outperforms all comparative models and can be used effectively for forecasting crude oil prices.

INDEX TERMS Crude oil price, feature selection, interval forecasting, multi-objective sparrow search algorithm, multivariate mixed-frequency combinatorial forecasting framework.

I. INTRODUCTION

Crude oil is a vital energy resource widely used in fuel, chemical, and industrial forecasting. The development of the global economy and the increase in energy demand have affected the crude oil price market, making it critical for industry and investors to understand crude oil market dynamics and trends [1]. Volatility in crude oil prices also has far-reaching implications for the global economy. Higher prices can lead to higher energy costs, exacerbating

The associate editor coordinating the review of this manuscript and approving it for publication was Essam A. Rashed.

inflationary pressures and negatively impacting consumers and businesses. Conversely, a price drop can boost the economy, lower energy costs, and promote economic growth [2]. In summary, effective crude oil price forecasting is essential for business decision-making, investment decisions, policy formulation, and economic impact assessment [3], [4]. However, crude oil prices are affected by many external factors, such as the geopolitical situation, economic growth, monetary policy, etc. [5], and there are also many uncertainties in the crude oil market, such as political unrest, natural disasters, technological breakthroughs, etc. [6], [7]. These complex factors make the fluctuation of crude oil prices nonlinear and unstable [8], which makes accurate forecasting of crude oil prices a problematic task. To stabilize the global economy and reduce risks in the energy market, the development of accurate and reliable models to forecast the price of crude oil has become a focus of global attention.

TABLE 1. Abbreviations.

GRB	combined model of GRU, RBF, and BPNN
MOSSA	Multi-Objective Sparrow Search Algorithm
ICEEMDAN	Improved Complete Ensemble Empirical Mode Decomposition with Adaptive Noise
BPNN	Back Propagation Neural Network
RBF	Radial Basis Function Neural Network
GRU	Gated Recurrent Unit
Elman	Elman Neural Network
ELM	Extreme Learning Machine
RNN	Recurrent Neural Network
biLSTM	bi-directional Long Short-Term Memory
MSSA	Multi-objective Salp Swarm Algorithm
MODA	Multi-Objective Dragonfly Algorithm
MALO	Multi-Objective Ant Lion Optimizer
RFE	Recursive Feature Elimination
MI	Mutual Information
VMD	Variational Mode Decomposition
EEMD	Ensemble Empirical Mode Decomposition
CEEMD	Complementary Ensemble Empirical Mode Decomposition
CEEMDAN	Complementary Ensemble Empirical Mode Decomposition with Adaptive Noise
MSE	Mean squared error
MAE	Mean absolute error
RMSE	Root mean square error
MAPE	Mean absolute percentage error
E-lm	The legates and mcCabe index
r	Correlation coefficient
FINAW	Normalized averaged width of the forecast interval
AWD	Accumulated width deviation
FICP	Coverage probability of the forecast interval
AIS	Average interval score
CWC	Coverage width-based criterion

The innovations of this study can be summarized as follows.

- Collects several low-frequency data and several high-frequency impact factor data used as input characteristics in the crude oil price modeling process, and finally proposes a new multivariate mixed-frequency forecasting method for crude oil prices, which fills a gap in current research and has directional implications for related industries.
- Two feature selection methods (recursive feature elimination, mutual information) are introduced into the framework, which are used to select the low-frequency and high-frequency influencing factors, respectively, to provide suitable features for the designed crude oil price forecasting framework.
- The method, which simultaneously considers the impact of multiple low-frequency influence factors and a high-frequency influence index on the crude oil price forecast, overcomes the previous limitation of considering only co-frequency influence factors.
- The MOSSA optimization algorithm is used to combine the forecast results of three models, GRU, RBF, and BPNN, to obtain optimal combined forecast results.

This study is organised as follows. Section II is a literature review. Section III is an introduction to the model and methodology. Section IV describes the proposed combined forecasting system. In Section V, some numerical experiments and analysis are conducted. Section VI contains some discussions. Section VII is the conclusion.

II. REVIEW OF LITERATURE

Several crude oil price forecasting methods have been developed, namely statistical models [9], artificial intelligence methods [10], [11], and combined forecasting methods [12], [13].

A statistical model is a method that uses historical data and statistical methods to forecast crude oil prices. Commonly used statistical models include regression models [14], time series models [15], [16], and cointegration models [17]. For example, Mohammadi et al. [18] examined several ARIMA-GARCH models for modelling and forecasting weekly crude oil spot prices in the international market. They found that the APARCH model performed best in most cases. Although statistical models have some applications in predicting crude oil prices, price changes may have nonlinear relationships, while statistical models usually assume that the relationship between variables is linear. As a result, statistical models need help capturing the complexity and nonlinear trends in price changes, which can lead to inaccurate prediction results. Therefore, statistical models need to provide satisfactory forecasting performance.

With the advent of artificial intelligence and its rapid development, methods for predicting crude oil prices have also evolved rapidly. These methods mainly include neural networks (such as PNN [19], BPNN [20]. RBFNN [21]), deep learning (for example, GRU [22], LSTM [23], etc.), machine learning (such as SVM [24], Random Forest [25], etc.). For example, [26] Yin and Wang studied the forecasting of daily WTI crude oil prices using chaos theory and artificial intelligence techniques (ANN). They analyzed the effects of noise on price forecasting. Liang et al. [27] developed a novel deep reinforcement learning algorithm for multilevel crude oil price forecasting. These studies have shown that despite the potential of AI methods for crude oil price forecasting,

there are some drawbacks and challenges. For example, AI can encounter problems such as overfitting and local optimization, often resulting in crude oil price forecasting failing to achieve the desired results.

To address the shortcomings of a single artificial intelligence model and integrate the advantages of the models, combined forecasting systems that combine two or more existing methods have been proposed and applied to time series forecasting, and the forecasting results have been significantly improved [28]. Li et al. [29] achieved improved forecasting performance using a data preprocessing method (ICEEMDAN), state space correlation entropy (SSCE), and a kernel-based extreme learning machine improved by the Gorilla Troop Optimization Algorithm (GTO-KELM). Jiang et al. [30] proposed a new forecasting framework for electricity prices that considers the effects of multiple variables on the forecasting results and realizes multiple inputs and outputs. The results of point and interval forecasts can be output simultaneously. Therefore, these hybrid models under study can fully exploit the features and advantages of different models to improve the completeness of forecasts [31].

In recent years, although many combined forecasting systems have been proposed, most consider only a single variable and need to fully account for the effects of different factors on the forecast. To fill this gap, Jiang et al. [32] proposed a new multidimensional forecasting system for electricity prices using multivariate and multiple-input-multiple-output structures. However, if too many variables are entered, this leads to redundancy in the model, increasing the computational cost of the model. Thus, the runtime, so selecting appropriate variables, is also an important focus in research [33]. In addition, feature selection plays an essential role in machine learning. It improves model performance, reduces the risk of overfitting, improves interpretability, and helps us better understand and use the data [34]. Therefore, feature selection methods are often used to select appropriate variables [35]. Among them, the RFE algorithm is known for its great advantages in systematically analysing and determining the best feature set by iteratively eliminating irrelevant features. It has been proven that the RFE algorithm performs better and more efficiently in this area than other feature selection methods. Its unique capabilities make it a reliable tool for finding the best feature set and an effective method for feature selection. RFE is suitable for datasets with a high number of features and where high accuracy forecasts are required [36], [37]. Mutual information directly measures the extent to which a trait contributes to a target variable based on information gain. It allows for greater adaptability to data and a more comprehensive consideration of feature relationships in feature selection. Mutual information is suitable for datasets with complex data distribution and insignificant relationships between features [38]. For example, Wang et al. [39] has developed a novel multivariate hybrid forecasting system by combining mixed signal preprocessing techniques, feature selection methods (random forest algorithms), deep learning models, neural network models, and population intelligence optimization strategies. Urolagin et al. [40] used selectKBest and correlation analysis for feature selection. Six MLSTM models were constructed for crude oil price forecasting using different features, transformations, and outlier elimination. The results show that selecting appropriate features can reduce model redundancy and increase the accuracy of model forecasting.

These models introduced multivariate variables to overcome the limitations of a single variable, but the lack of one ignores the effects of mixed-frequency on prediction results [41]. In particular, mixed-frequency data includes both high-frequency and low-frequency data, so that forecasts based on mixed-frequency data can achieve better results than those based solely on data with the same frequency, as they take full advantage of the real-time and informational nature of the high-frequency data and the global trend of the low-frequency data. This combined use of data at different frequencies helps to improve the accuracy and scope of forecasts [42]. Mixed-frequency data can synthesize information from different time scales, improve forecast accuracy, account for seasonal and cyclical factors, deal with nonlinear relationships, and provide more comprehensive forecasts and decision support. As a result, the hybrid frequency approach has become a valuable tool for forecasting crude oil prices [43], [44]. Example, Hao et al. [45] developed a new mixed-frequency forecasting model by taking advantage of the mixed-frequency method to improve the forecasting accuracy and performance of the model. Degiannakis and Filis [46] conducted real out-of-sample forecasts of monthly oil futures prices using daily volatilities and returns from financial and commodity markets. It was found that using mixed frequency data significantly improved the prediction of oil prices and reduced the mean squared error by about 68%. This suggests that using a combination of high frequency and low frequency data can significantly improve oil price forecasting and is an effective means of predicting market trends more accurately. In summary, the mixed-frequency approach can integrate and analyze data from different time scales and better capture the nonlinear fluctuations in crude oil prices. This helps improve forecast accuracy and brings the results closer to the actual situation.

However, most researchers design combined models that consider either a single variable [47] or only the co-frequency variables, ignoring the importance of the mixed frequency [48]. Therefore, this paper proposes a multivariate, mixed-frequency, combined forecasting method that simultaneously considers several low-frequency influences and a high-frequency influence index to obtain accurate forecasts for crude oil price points and intervals.

III. MODEL INTRODUCTION

A. DATA PREPROCESSING

The ICEEMDAN signal processing method proposed by Colominas et al. is an improvement of CEEMDAN [49].

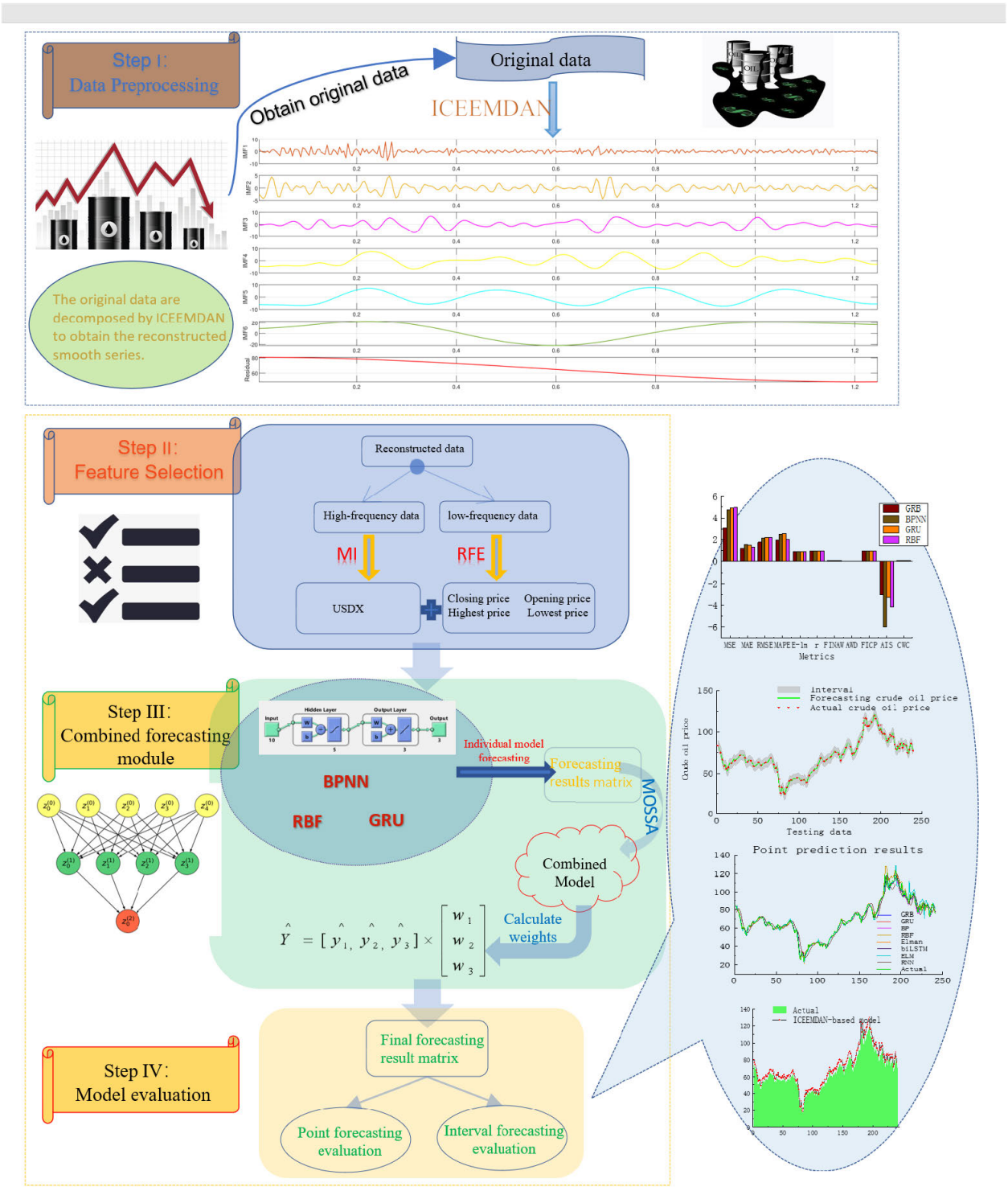

FIGURE 1. Flowchart of the proposed system.

ICEEMDAN is improved by introducing adaptive noise tuning, which reduces modal aliasing and artifacts by dynamically adjusting the noise intensity based on the frequency and amplitude information of the IMFs. This enables a more accurate signal decomposition and improves the quality and reliability of the IMFs.It provides a more accurate and reliable basis for subsequent analysis, modeling, and forecasting.

ICEEMDAN is a powerful signal analysis method mainly used to deal with nonlinear and non-stationary signals [50]. Its function is to extract intrinsic patterns and trends from complex signals while eliminating possible noise interference, thereby improving the accuracy and reliability of signal analysis [51]. ICEEMDAN has good adaptive capabilities and can automatically adjust processing parameters to adapt to changes in different data characteristics. At the same time, it does not rely on future information, helping to avoid forward-looking bias [52]. It is significant for analyzing complex signals such as time series and image data and provides strong support for data analysis and pattern recognition.

The ICEEMDAN method can be used to deal with the nonlinear and non-stationary characteristics of crude oil prices and extract important patterns such as trends, periodicities, and mutation points in price time series while effectively removing noise interference, thereby improving the performance of the forecast model stability and accuracy [53]. Its adaptability and independence from future information enable it to better cope with the volatility and complexity of the crude oil market, improve the forecasting model's ability to capture price changes and provide important decision support for investors and related institutions. and market forecast basis [29].

In this study, ICEEMDAN is mainly used to decompose crude oil price data into multiple IMFs, each representing vibration modes on different time scales. Finally, the noise sequence is removed, and the remaining sequence is reconstructed to obtain more stable data. Thereby improving the stability and accuracy of the forecast model. The details are as follows: Taking the decomposition of the crude oil closing price series as an example, the steps are: Assume X is the original series and $(E_k \cdot)$ is the kth mode of the EMD decomposition method.

STEP 1: ADD WHITE GAUSSIAN NOISE $\Phi^{(I)}$ TO THE ORIGINAL SIGNAL X AND CONSTRUCT SEQUENCES $X^{(I)}$

$$X^{(i)} = X + \varepsilon_0 E\left(\Phi^{(i)}\right), \tag{1}$$

where ε_0 is the amplitude coefficient of the added noise.

STEP 2: CALCULATE THE FIRST RESIDUAL

$$R_1 = \left[N\left(X^{(i)}\right)\right], \tag{2}$$

where $N(\cdot)$ is an operator that generates the local mean.

STEP 3: CALCULATE THE FIRST MODE COMPONENT IMF_1

$$IMF_1 = X - R_1. \tag{3}$$

STEP 4: CALCULATE THE SECOND MODE COMPONENT IMF_2

Calculate the second residual: $R_2 = R_1 + \beta_1 E\left(\Phi^{(i)}\right)$, and calculate IMF_2 based on the (4):

$$IMF_2 = R_1 - R_2. \tag{4}$$

STEP 5: CALCULATE THE FIRST MODE COMPONENT IMF_K

Calculate the k-th residual:$R_K = \left[N\left(R_{k-1} + \varepsilon_{k-1} E\left(\Phi^{(i)}\right)\right)\right]$. Calculate IMF_k based on (5):

$$IMF_k = R_{k-1} - R_k. \tag{5}$$

Step 6: Until all modal components and residuals are computed and decomposed. Then the noise series is deleted and the remaining subsequence is reconstructed to obtain the preprocessed data series, The formula is shown in (6):

$$\widetilde{x}(t) = \sum_{k=2}^{n} IMF_k(t) \tag{6}$$

where n is the number of IMFs.

B. FEATURE SELECTION MODEL

Proper selection of influential features can reduce model complexity and improve prediction accuracy while reducing training time. The data collected in this work has a variety of features, and it is necessary to search for appropriate input features to reduce the complexity of the forecasting model and avoid overfitting the model. In the proposed model, the influence of both low-frequency data features and high-frequency influencing factors on the model is considered. Specifically, a recursive feature elimination method is applied to determine the low-frequency influence factor, and the optimal high-frequency influence factor is selected based on the mutual information.

1) RECURSIVE FEATURE ELIMINATION (RFE)

RFE is a feature selection method based on machine learning (In this study the choice was based on Support Vector Regression (SVR)) [54]. Unlike other feature selection methods, recursive feature elimination trains a model and then gradually removes unnecessary features based on the importance of the feature. Where SVR is to find the best estimated function f(x) corresponding to the crude oil price series:

$$f(x) = \varpi^T \psi(x) + b, \tag{7}$$

$\psi(x)$ is a nonlinear mapping from the input feature space to the high-dimensional feature space, ϖ is the weight vector and b is the bias.

Suppose there are N training samples, then $\{(x_i, y_i)|i=1, 2, \cdots, N\}$, x_i is the feature expression matrix to be selected and y_i is the crude oil price sequence. The steps of the algorithm are defined as follows:

1) Train the SVR model to obtain the weights ϖ;
2) Calculate the ranking score using the formula $\kappa_i = \varpi_i^2$;
3) Remove the feature with the lowest score;
4) Repeat steps 1)-3) until the standard number of features to keep is reached.

There are two approaches to recursive feature elimination: bottom-up and top-down. The bottom-up approach starts with a single feature and gradually increases the number of features to be selected. The top-down approach starts with

the original feature set and gradually reduces the number of features to be selected. In this study, a top-down approach was used.

2) MUTUAL INFORMATION (MI)

Mutual information (MI) measures the interdependence between variables and can be used for feature selection [55]. MI measures the degree of information exchange between two variables and, therefore, can be used to evaluate the relationship between input features and output targets. The specific description of MI is as follows:

Consider a scenario where the joint distribution of two random variables (X, Z) is represented as p(x, z), with individual marginal distributions as p(x) and p(z). The mutual information $MI(X;Z)$ represents the relative entropy between the joint and marginal distributions and is expressed as follows:

$$MI(X;Z)=\sum_{z\in(Z)}\sum_{x\in(X)}p(x,z)\log\frac{p(x,z)}{p(x)p(z)}, \tag{8}$$

where the logarithm function is usually based on 2 or the natural base.

The main steps of MI are as follows:

1) Calculate the value of mutual information between the target variable and each feature;
2) Sort the features according to the magnitude of mutual information;
3) Selecting the best-valued features as input features.

The larger the value of the mutual information, the closer the relationship between the two random variables. If the mutual information equals 0, there is no relationship between X and Z.

C. BENCHMARK MODELS

1) BPNN

A BP neural network (BPNN) is a common artificial neural network used for supervised learning tasks in which the input signal is passed to the output layer by forward propagation and the weights are adjusted to minimise the error between the predicted output and the actual output by backward propagation [56]. The calculation process is as follows [45]: The output values of the hidden layer and output layer can be represented as:

$$x_j^{[l]}=\sigma_j^{[l]}\left(\sum_{k=1}^{n}x_k^{[l-1]}w_{kj}^{[l]}+\theta_j^{[l]}\right). \tag{9}$$

The node error of the output layer is shown below:

$$E=\frac{1}{2}\sum_k\left(T_j-\sigma_1^{[2]}\left(\sum_i x_j^{[l]}w_{k1}^{[2]}+\theta_j^{[l]}\right)\right)^2. \tag{10}$$

The correction of the connection weights can be represented as:

$$\triangle W_{nj}=-\eta\partial E/\partial W_{nj}. \tag{11}$$

The threshold correction is represented as:

$$\triangle\theta_j^{[l]}=-\eta\partial E/\partial\theta_j^{[l]}. \tag{12}$$

In the above equation, $x_j^{[l]}$ represents the output value of the jth neuron node in the l layer; X_j (j=1, 2,…, j) can be considered as a particular case of, $x_j^{[l]}$ at layer 0; $\sigma_j^{[l]}$, $\theta_j^{[l]}$, T_j are the activation function, threshold, and output expectation of the jth node in the l layer, respectively; $w_{kj}^{[l]}$ is the connection weight between n nodes and j nodes in the first layer, and η is the learning rate.

2) RBF

A radial basis function (RBF) neural network belongs to the type of feedforward neural network, which is a three-layer feedforward network. RBF neural networks have excellent performance in handling nonlinear problems and function fitting. In real-world simulation experiments, the positive definite Gauss function is usually chosen as the RBF hidden layer function [57], as shown in (13).

$$P_j=\exp\left(-\frac{|x-c_j|^2}{2\delta_j^2}\right). \tag{13}$$

where, x denotes the input sample, P_j represents the node vector of the hidden layer, and c_j stands for the center vector of the hidden layer node, sharing the same dimension as the input sample. Additionally, δ_j signifies the width of the hidden layer node. The linear output expression of RBF is:

$$y(x)=\Sigma_{j=1}^{n}w_jP_j. \tag{14}$$

where y is the calculated output value of the neural network, and n is the number of hidden layer neuron nodes; W_j represents the weight between the hidden layer and the output layer.

3) GRU

The GRU network is a variant of the traditional recurrent neural network. It is suitable for processing and forecasting long-term dependence problems of dynamic nonlinear sequences such as time series. Compared to the three-port structure of the LSTM neural network, it controls the storage and update of sequential data by a two-port structure with update and reset ports. This reduces memory requirements and enables faster execution. The GRU network controls the degree of integration with historical moments through the reset gate ξ_t, and the update gate ϖ_t controls the degree of memory data retention. The calculation process is shown in the following equation [58]:

$$\boldsymbol{\xi_t}=\varrho\left(\boldsymbol{W_\xi}\cdot[\boldsymbol{\kappa}_{t-1},\boldsymbol{x}_t]+\boldsymbol{\vartheta}_\xi\right) \tag{15}$$

$$\boldsymbol{\varpi}_t=\varrho\left(\boldsymbol{W}_\varpi\cdot[\boldsymbol{\kappa}_{t-1},\boldsymbol{x}_t]+\boldsymbol{\vartheta}_\varpi\right) \tag{16}$$

$$\widetilde{\boldsymbol{\kappa}_t}=\tanh\left(\boldsymbol{W}_\kappa\cdot\left[\boldsymbol{\xi}_t\boldsymbol{\kappa}_{t-1},\boldsymbol{x}_t\right]+\boldsymbol{\vartheta}_\kappa\right) \tag{17}$$

$$\boldsymbol{\kappa}_t=(1-\boldsymbol{\varpi}_t)\,\boldsymbol{\kappa}_{t-1}+z_t\widetilde{\boldsymbol{\kappa}_t} \tag{18}$$

where $\varrho(.)$ is the Sigmoid function, W_ξ and ϑ_ξ are the reset gate weight and offset, W_ϖ and ϑ_ϖ are the update gate weight

and offset, W_κ and ϑ_κ are The weight and offset of the tanh neural layer, x_t is the time series input at the current moment, and κ_{t-1} is the hidden state at the previous moment.

D. MOSSA

The multi-objective sparrow search algorithm (MOSSA) was developed by Xue and Shen [59]. In the mathematical modeling, the sparrow population foraging was divided into discoverers and joiners, and a detection and warning mechanism was also added. Individuals among the sparrows that find food better act as discoverers, and others act as finders. In contrast, some individuals are selected for detection and warning and give up feeding when a threat is detected. The mathematical modeling process is described in detail below:

1) MATHEMATICAL MODELING

In the mathematical modeling, we use virtual sparrows for foraging, and the definition of a sparrow population can be expressed as follows:

$$Y = \begin{bmatrix} y_{1,1} & x_{1,2} & \cdots & y_{1,n} \\ y_{2,1} & y_{2,2} & \cdots & y_{2,n} \\ \vdots & \vdots & \vdots & \vdots \\ y_{k,1} & y_{k,2} & \cdots & y_{k,n} \end{bmatrix}, \tag{19}$$

where n is the dimension of the problem variable to be optimized, and k is the number of sparrows.

The calculation of the fitness value for each sparrow is shown below:

$$F_y = \begin{bmatrix} f\left(\left[y_{1,1}\ y_{1,2}\ \cdots\ y_{1,n}\right]\right) \\ f\left(\left[y_{2,1}\ y_{2,2}\ \cdots\ y_{2,n}\right]\right) \\ \vdots \\ \vdots \\ f\left(\left[y_{k,1}\ y_{k,2}\ \cdots\ y_{k,n}\right]\right) \end{bmatrix}, \tag{20}$$

where f is the fitness value.

The algorithm categorizes sparrows into discoverers, joiners, and scouts. The discoverers are responsible for finding food and providing foraging directions to all joiners. The position of the discoverers is updated with the following formula:

$$Y_{i,j}^{t+1} = \begin{cases} Y_{i,j}^{t} \cdot exp\left(-\dfrac{i}{\beta \cdot item_{max}}\right) & R_2 < T \\ Y_{i,j}^{t} + Q \cdot L & R_2 > T. \end{cases} \tag{21}$$

where t denotes the current iteration number, j=1,2,3,...,n. $item_{max}$ signifies the maximum number of iterations. $Y_{i,j}^{t}$ represents the position information of the ith sparrow at the jth dimensional iteration number t. Additionally, $\beta \in (0, 1]$ is a random number, $R_2 \in [0, 1]$ and $T \in [0.5, 1]$ denote the warning value and the safety value, respectively. Q is a random number following a normal distribution, while L denotes a $1 \times n$ matrix with all elements being 1.In the event that $R_2 < T$, it implies the absence of nearby predators, prompting the searcher to conduct an extensive exploration. Conversely, if $R_2 \geq T$, the presence of a predator triggers an immediate alarm, prompting all sparrows to change their foraging positions instantly.

The formula for updating a joiner position is as follows:

$$Y_{i,j}^{t+1} = \begin{cases} Q \cdot exp\left(\dfrac{X_{worst}^{t} - Y_{i,j}^{t}}{i^2}\right) & i > \dfrac{k}{2} \\ Y_{p}^{t+1} + \left|Y_{i,j}^{t} - X_{p}^{t+1}\right| \cdot B^{+} \cdot L & i \leq \dfrac{k}{2}. \end{cases} \tag{22}$$

Y_p^{t+1} is the optimal position currently occupied by the discoverers, and Y_{worst} denotes the current global worst position. B denotes a $1 \times d$ matrix, where each element is randomly assigned a value of 1 or -1, and $B+ = B^{\top}(BB^{\top})^{-1}$. If $i \leq \frac{k}{2}$, the joiner will follow the discoverer toward a better foraging location; when $i > \frac{k}{2}$, this suggests that the ith joiner with the lower fitness value did not receive food and is starving; at this point, it needs to fly elsewhere to forage for more energy.

The scout is responsible for the safety of the sparrow and immediately sends an alarm signal when it detects a predator. At that time, the sparrow will directly engage in anti-predator behavior to ensure its safety. The updated formula for scouts is as follows:

$$Y_{i,j}^{t+1} = \begin{cases} Y_{best}^{t} + \gamma \cdot \left|Y_{i,j}^{t} - Y_{best}^{t}\right| & f_i > f_M \\ Y_{i,j}^{t} + C \cdot \left(\dfrac{\left|Y_{i,j}^{t} - Y_{worst}^{t}\right|}{(f_i - f_m) + \delta}\right) & f_i = f_M. \end{cases} \tag{23}$$

Y_{best}^{t} denotes the current globally optimal foraging position, while γ is a normally distributed random number utilized for controlling the step size. C represents a constant within the range of $[-1, 1]$, and f_i stands for the current fitness value of each individual sparrow. Furthermore, f_M and fm refer to the current global optimal and worst fitness values, respectively. δ is a smaller constant number whose function ensures that the denominator is not zero. If $f_i > f_M$, means that the sparrows are in the dangerous location, and if $f_i = f_M$, This implies that the sparrow located in the middle of the population is conscious of potential danger and should maintain proximity to other sparrows in order to minimize the risk of being hunted.

2) MODEL COMBINATION PROBLEM CONSTRUCTION

To overcome the limitations of each model and integrate their advantages. It is necessary to optimize them with multiple objectives. Considering the stability and accuracy of the model, three error indicators, MAPE, RMSE, and FICP, are selected as objective functions for combining models with the

TABLE 2. Dataset description.

Dataset	Frequency	Variables	Samples	Size	Statistical indicators				
					Max	Min	Std	Average value	Median
WTI	Weekly	Closing price	Total samples	1200	145.29	16.94	25.81	63.34	60.58
			Training	960	145.29	18.00	26.87	62.84	59.89
			Testing	240	120.67	16.94	20.99	63.36	62.23
	Weekly	Opening price	Total samples	2000	144.69	16.84	25.87	63.34	60.61
			Training	960	144.69	18.05	26.90	62.81	59.90
			Testing	240	121.33	16.84	21.15	65.46	62.01
	Weekly	Highest price	Total samples	1200	147.27	18.26	26.46	65.50	62.52
			Training	960	147.27	19.25	27.46	64.85	61.95
			Testing	240	130.50	18.26	21.86	68.11	64.20
	Weekly	Lowest price	Total samples	1200	139.17	-40.32	25.24	60.87	58.69
			Training	960	139.17	16.70	26.24	60.57	58.04
			Testing	240	117.14	-40.32	20.79	62.07	60.12
Brent	Weekly	Closing price	Total samples	1200	144.49	17.75	29.11	66.74	63.80
			Training	960	144.49	17.75	30.76	65.85	61.95
			Testing	240	122.01	21.44	20.98	70.31	68.34
	Weekly	Opening price	Total samples	1200	144.4	17.4	29.13	66.70	63.74
			Training	960	144.40	17.40	30.76	65.79	61.82
			Testing	240	122.79	21.55	21.07	70.32	68.47
	Weekly	Highest price	Total samples	1200	147.5	18.7	29.72	68.80	65.80
			Training	960	147.50	18.70	31.30	67.74	63.68
			Testing	240	139.13	27.88	21.84	73.04	70.35
	Weekly	Lowest price	Total samples	1200	139.54	15.98	28.38	64.39	61.46
			Training	960	139.54	16.65	30.10	63.69	59.51
			Testing	240	118.55	15.98	19.87	67.19	65.68
USDX	Daily	USDX price	Total samples	6000	121.21	71.30	11.22	91.52	90.75
			Training	4800	121.21	71.30	11.81	90.03	87.42
			Testing	1200	114.05	89.31	5.23	97.48	96.59

following details in this paper:

$$Min \begin{cases} MAPE = \dfrac{1}{N}\sum_{i=1}^{N}\left|\dfrac{T_i - \tilde{T}_i}{T_i}\right| \cdot 100\% \\ RMSE = \sqrt{\dfrac{1}{N}\cdot\sum_{i=1}^{N}\left(T_i - \tilde{T}_i\right)^2} \\ FICP = \dfrac{1}{N}\sum_{i=1}^{N}\alpha_i \\ \alpha_i = \begin{cases} 1, & T_i \in [\underline{p}^t, \bar{p}^t] \\ 0, & T_i \notin [\underline{p}^t, \bar{p}^t]. \end{cases} \end{cases} \tag{24}$$

where T_i and $\tilde{T}_i$ are the actual and forecasting values of the variables, respectively. N is the length of the forecasting series. $\bar{p}^t$ and $\underline{p}^t$ are the upper and lower bounds of the forecasting interval.

IV. CONSTRUCTION OF COMBINED FORECASTING SYSTEM

The system considers several low-frequency factors (weekly data) and a high-frequency impact index (daily data) for weekly closing price forecasts of crude oil futures and can output both point and interval forecasts at the same time. The system includes four stages: the data noise reduction module, the feature selection module, the combined forecast module, and the evaluation module. The flowchart of the system is shown in Fig 1.

A. DATA DESCRIPTION

1) WEEKLY DATA

In this study, intercontinental Exchange is used as the research object. WTI crude oil is selected as WTI, and Brent crude oil is selected as Brent to conduct experiments and test the performance of the system. Each dataset contains a set of crude oil futures closing prices, a set of crude oil futures opening prices, a set of crude oil futures lowest price, a set of crude oil futures highest price, a set of crude oil futures trading volume, and a set of crude oil futures rise and fall. The sampling frequency is weekly, and the sampling period is 2010.01.01-2023.05.01; each data set contains 1200 data points. The data are divided into training and testing data, and the ratio between training and testing data is 4:1.

2) DAILY DATA

When considering the impact indices, we collected a total of three indices: US Dollar Index® (USDX), Dow Jones Index (US 30), and S&P 500 Index (US 500). The sampling frequency is daily, and the sampling period is from

01/01/2010 to 05/05/2023. Each dataset contains 6000 data points. More detailed information is provided in Table 2.

B. DATA NOISE REDUCTION MODULE

Noise is reduced to obtain smooth time series data, which provides a more accurate and reliable basis for subsequent analysis and forecasting. ICEEMDAN was used to decompose and reconstruct the original data. The collected weekly and daily data are pre-processed separately with ICEEMDAN. In particular, crude oil price series are used here as an example, where the crude oil price series are decomposed into a series of IMFs and high-frequency IMF_s are eliminated to filter out noise. Here, IMF_1 is usually considered as a high-frequency IMF, and the residuals $\{IMF_2, IMF_3 \cdots IMF_S\}$ are reconstructed to obtain the final sequence. The same reconstruction was performed for the other sequences. Details on ICEEMDAN are in section III-A.

C. FEATURE SELECTION MODULE

1) WEEKLY DATA FEATURE SELECTION

Since the weekly crude oil data collected in this study have multiple features, it is necessary to philter out the appropriate input features to reduce the complexity of the model and the risk of overfitting. In particular, recursive feature elimination is used to select appropriate features. Each dataset contains six features, and according to the recursive feature elimination strategy, four more essential features finally remain in each dataset. The RFE in this study is based on a SVR to achieve feature selection, so the selection method is based on the importance of each feature in the decision tree to select the appropriate variable. The feature selection results are shown in Table 3, where ✓ indicates that the feature was selected and × indicates that the feature was not selected. The results show that the closing price, opening price, highest price, and lowest price were selected as input variables for both data sets. Therefore, the inputs of the low frequency variables are $\{x_{t-4}, x_{t-3}, x_{t-2}, x_{t-1}, x_t$, opening price, highest price, lowest price$\}$, where x_t is the baseline characteristic of week t.

TABLE 3. Low-frequency feature selection for two datasets.

Dataset	Variable	Choose or not
WTI	Closing price	✓
	Opening price	✓
	Highest price	✓
	Lowest price	✓
	Trading volume	×
	percentage rise or fall in price	×
Brent	Closing price	✓
	Opening price	✓
	Highest price	✓
	Lowest price	✓
	Trading volume	×
	percentage rise or fall in price	×

2) DAILY INDEX FEATURE SELECTION

This study also examined the impact of high-frequency indices on crude oil prices, considering three indices: USDX, US 30, and US 500. To select the most important indexes, the mutual information method is used to select appropriate high-frequency indexes. The value of MI reflects the importance of the index, the appropriate variable is selected based on the size of the MI value, and the larger the value of MI, the more influential the feature is. The ranking of the importance of the high-frequency influence index is shown in Table 4, and the results show that USDX was selected for both data sets. Since the closing prices of crude oil futures are not open on weekends, only the data from Monday to Friday corresponding to the weekly crude oil prices to be forecast are used as high-frequency input variables. That is, the inputs to the high-frequency impact index are $\{USDX_1^t, USDX_2^t, USDX_3^t, USDX_4^t, USDX_5^t\}$, where $USDX_j^t$ represents the daily data for the jth day of the t-th week.

TABLE 4. High-frequency feature selection for two datasets.

Dataset	Index futures	MI value	Ranking order
WTI	USDX	0.8309	1
	US 30	0.7636	2
	US 500	0.6661	3
Brent	USDX	0.8556	1
	US 30	0.8153	2
	US 500	0.6825	3

D. COMBINED PREDICTION MODULE

1) SINGLE MODEL FORECASTING

The denoised data are divided into a training set and a test set in a 4:1 ratio, with 960 (1-960) training sets, 240 (961-1200) test sets for low-frequency variables, and 4800 (1-4800) training sets and 1200 (4801-6000) test sets for high-frequency variables. Specifically, GRU, RBF, and BPNN models are used to obtain point and interval forecasts. The prediction model of the dataset determines that the input variables $\{x_{t-4}, x_{t-3}, x_{t-2}, x_{t-1}, x_t$, opening price, highest price, lowest price, $USDX_1^t$,$USDX_2^t$,$USDX_3^t$,$USDX_4^t$,$USDX_5^t\}$, and the output variables are $\{\underline{c}^t, c^t, \bar{c}^t\}$, where $\underline{c}^t$, c^t and $\bar{c}^t$ are the upper bound, lower bound, and point value of the interval forecast at time t, respectively. The estimation of the interval forecast is shown in (25). The detailed input structure is shown in (26), and the output structure is shown in (27).

$$\left[\underline{c}^t, \bar{c}^t\right] = \left[c^{t+1} - \mu \cdot \frac{s_c}{\sqrt{n}},\ c^{t+1} + \mu \cdot \frac{s_c}{\sqrt{n}}\right]. \tag{25}$$

where s_c and n are the standard deviations of the predicted values of crude oil price points, and the number of predicted samples, respectively, μ is the interval coefficient. (26), as shown at the bottom of the next page, where O_t, H_t, and L_t denote the opening, highest and lowest prices of crude oil futures in week t. U_i^t denotes US Dollar Index® (USDX)

corresponding to day i (i=1,2,...,5) of week t. X denotes the output characteristic.

$$\Downarrow$$
$$\textit{output matrix}$$
$$\begin{bmatrix} X_{(t+1)low} & X_{t+1} & X_{(t+1)up} \\ X_{(t+2)low} & X_{t+2} & X_{(t+2)up} \\ \vdots & \vdots & \vdots \\ X_{(n)low} & X_n & X_{(n)up} \end{bmatrix} \tag{27}$$

X_{low}, X_{up} denote the lower and upper bounds of the interval forecast, respectively, and X_t represents the forecast value at week t.

2) MODEL COMBINATION

In this study, the model combination is performed using the MOSSA algorithm. Since the proposed forecasting framework provides both point and interval forecasts, the role of MOSSA in both point and interval forecasts is to compute the combined weights of the three base forecasting models (GRU, RBF and BPNN), i.e. 240 forecasts are derived as a validation set using the three individual models to compute their optimal combined weights by MOSSA, which are then combined to obtain the final forecasts. The final result can be calculated using (28):

$$\tilde{P}_{final} = \omega_1 \cdot \tilde{P}_1 + \omega_2 \cdot \tilde{P}_2 + \omega_3 \cdot \tilde{P}_3. \tag{28}$$

where ω_i and $\tilde{P}_i$, i=1,2,3 are the weights and prediction results of the member model, respectively.

E. EVALUATION MODULE

To validate the performance of the developed combined forecasting model, six-point forecast and five-interval forecast evaluation indicators are used in this study.

1) POINT FORECASTING EVALUATION

The six-point forecast evaluation indicators are MSE, MAE, RMSE, MAPE, E-lm and r. Among them, MSE, MAE, RMSE, and MAPE, the smaller value of these four metrics also indicates better forecasting performance. In addition, the correlation coefficient (r) is used to examine the degree of linear correlation between variables. Another measure of predictive accuracy is E-1m, which also measures correlation. r and E-lm have higher values, indicating better performance of the predictive model. A detailed description of the evaluation measures used in this study can be found in Table 5.

TABLE 5. Point forecasting evaluation metrics.

Metrics	Equation
MSE	$\frac{1}{N}\sum_{i=1}^{N}\left(T_i-\tilde{T}_i\right)^2$
MAE	$\frac{1}{N}\sum_{i=1}^{N}\left\|T_i-\tilde{T}_i\right\|$
RMSE	$\sqrt{\frac{1}{N}\cdot\sum_{i=1}^{N}\left(T_i-\tilde{T}_i\right)^2}$
MAPE	$\frac{1}{N}\sum_{i=1}^{N}\left\|\frac{T_i-\tilde{T}_i}{T_i}\right\|\cdot 100\%$
E-lm	$1-\sum_{i=1}^{N}\left\|\tilde{T}_i-T_i\right\| / \sum_{i=1}^{N}\left\|T_i-\bar{T}\right\|$
r	$\sum_{i=1}^{N}\left(T_i-\overline{T}\right)\left(\tilde{T}_i-\overline{\tilde{T}}\right) / \sqrt{\sum_{i=1}^{N}\left(T_i-\overline{T}\right)\sum_{i=1}^{N}\left(\tilde{T}_i-\overline{\tilde{T}}\right)}$

Here, T_i and $\tilde{T}_i$ are the actual and predicted values of the variables, respectively, and $\overline{T}$ denotes the mean of the values. N is the length of the prediction series.

2) INTERVAL FORECASTING EVALUATION

The five interval evaluation metrics are FINAW, FICP, AWD, AIS, and CWC. FICP and FINAW are two metrics that conflict with each other to some degree, as decreasing the width can decrease the target detection probability. Therefore, larger FICP values and smaller FINAW values provide the best results. In this paper, a coverage breadth-based criterion (CWC) is introduced to integrate coverage and narrowness of forecast intervals. Specifically, the CWC is compared at a significance level of 0.95. Smaller values of FINAW, AWD, and CWC, smaller absolute values of AIS, and larger values of FICP indicate better prediction models. The mathematical formula used to calculate the evaluation indicators used in this study is shown in Table 6.

The individual steps of the proposed combined forecasting framework are as follows:

Step 1: Decomposition and reconstruction of the collected weekly and daily data using ICEEMDAN.

Step 2: The data processed in Step 1 is subjected to feature selection, where the daily data is selected by RFE to select appropriate variables, and the RFE in this study is based on a decision tree to achieve feature selection. The weekly data are selected according to the MI value, and the appropriate variables are selected according to the size of the MI value.

Step 3: Crude oil price forecasting is conducted using three benchmark models, GRU, RBF and BPNN, to obtain the corresponding point and interval forecasting results. The

$$\textit{input matrix}$$
$$\begin{bmatrix} X_{t-4} & X_{t-3} & X_{t-2} & X_{t-1} & X_t & O_t & H_t & L_t & U_1^t & U_2^t & U_3^t & U_4^t & U_5^t \\ X_{t-3} & X_{t-2} & X_{t-1} & X_t & X_{t+1} & O_{t+1} & H_{t+1} & L_{t+1} & U_1^{t+1} & U_2^{t+1} & U_3^{t+1} & U_4^{t+1} & U_5^{t+1} \\ \vdots & \vdots & \vdots & \vdots & \vdots & \vdots & \vdots & \vdots & \vdots & \vdots & \vdots & \vdots & \vdots \\ X_{n-5} & X_{n-4} & X_{n-3} & X_{n-2} & X_{n-1} & O_{n-1} & H_{n-1} & L_{n-1} & U_1^{n-1} & U_2^{n-1} & U_3^{n-1} & U_4^{n-1} & U_5^{n-1} \end{bmatrix} \tag{26}$$

specific input and output structures of the models can be seen in (26) and (27).

Step 4: The forecast results obtained in Step 3 are combined and forecasted through MOSSA to obtain the final forecast results.

Step 5: The proposed model is evaluated using the corresponding evaluation metrics.

TABLE 6. Interval forecasting evaluation metrics.

Metrics	Equation
FINAW	$\frac{1}{N}\sum_{i=1}^{N}\frac{\overline{P}_i-\underline{P}_i}{T_{\max}-T_{\min}}\times 100\%$
AWD	$\frac{1}{N}\sum_{i=1}^{N}, AWD_i=\begin{cases}\frac{\underline{P}_i-T_i}{\overline{P}_i-\underline{P}_i}, T_i<\underline{P}_i\\ 0, \quad T_i\in\underline{P}_i\\ \frac{T_i-\underline{P}_i}{\overline{P}_i-\underline{P}_i}, T_i>\underline{P}_i\end{cases}$
FICP	$\frac{1}{N}\sum_{i=1}^{N}\alpha_i, \alpha_i=\begin{cases}1, & T_i\in[\underline{p}^t,\overline{p}^t]\\ 0, & T_i\notin[\underline{p}^t,\overline{p}^t]\end{cases}$
AIS	$\frac{1}{N}\sum_{i=1}^{N}AIS_i,$
	$AIS_i=\begin{cases}-2\psi\left(\overline{P}_i-\underline{P}_i\right)-4\left[\underline{P}_i-T_i\right] & T_i<\underline{P}_i\\ -2\psi\left(\overline{P}_i-\underline{P}_i\right) & T_i\in\left[\underline{P}_i,\overline{P}_i\right]\\ -2\psi\left(\overline{P}_i-\underline{P}_i\right)-4\left[T_i-\overline{P}_i\right] & T_i>\overline{P}_i\end{cases}$
CWC	$FINAW\left(1+\gamma e^{-\eta(FICP-\mu)}\right), \gamma=\begin{cases}0 & FICP\geq\mu\\ 1 & FICP<\mu\end{cases}$

$\underline{p}^t$ and $\overline{p}^t$ are the upper and lower bounds of the interval forecasting. α_i is the number of true values in the prediction interval. n is the number of test sets. T_{max} and T_{min} are the largest and smallest values of the target in the forecasting process. AWD_i is the deviation of the width of the prediction interval for each sample. η and μ are the penalty parameters. The confidence interval determines μ, e.g., if the confidence level is 95%, μ = 0.95.

TABLE 7. Parameter setting of the models.

Models	Parameter	Value or Function
GRU	Number of inputs layer nodes	13
	Number of hidden nodes	300
	Number of Output layer nodes	3
	State Activation Function	tanh
	Gate Activation Function	SIGMOD
	Learning rate	0.001
	Epochs	100
BPNN	Number of hidden nodes	5
	Activation function	SIGMOD
	Learning rate	0.1
	Epochs	200
RBF	Number of hidden nodes	5
	Activation function	Gaussian function
MOSSA	Iteration number	100
	Population size	100
	Optimizing parameter dimension	3
	Archive set	100
	The number of objective functions	3

V. EXPERIMENT

In this study, four comparative experiments were conducted to validate the forecasting performance of the developed combinatorial forecasting framework. To prevent random factors from influencing the forecasting results, each forecasting model is run ten times, and the average of the forecasting results is used as the final result. The parameter settings of the model are shown in Table 7.

A. EXPERIMENT I: COMPARISON OF THE GRB WITH THE THREE INDIVIDUAL MODELS

To demonstrate the advantages of the combined framework, the proposed combined forecasting model is tested against GRU, RBF, and BPNN in this paper. The detailed experimental results are shown in Table 8 - 9.

The analysis shows that GRB has good forecasting ability in both point and interval forecasting, confirming the effectiveness of the combined method. This is especially true for the point forecast. The MAPE values of this hybrid forecasting model in the two datasets are $MAPE_1^{GRB}=1.9657\%$ and $MAPE_2^{GRB}=1.8498\%$, which is an improvement of $0.1-0.5\%$ compared to the results of GRU, RBF, and BPNN. MSE values are $MSE_1^{GRB}=3.1107$ and $MSE_2^{GRB}=3.4824$, which is an improvement of 0.4-1.8 compared to GRU, RBF or BPNN results. For the other metrics, MAE_{12}^{GRB}, $RMSE_{12}^{GRB}$, r_{12}^{GRB} and $E-lm_{12}^{GRB}$, the optimal value is also obtained. This indicates that the forecasting accuracy of GRB is higher than that of other individual models.

In interval forecasting, the GRB model reaches the maximum value in both datasets, $FICP_1^{GRB}=0.9792$,$FICP_2^{GRB}=0.9875$. This shows the excellent performance of the developed model for interval forecasting. For the interval forecasting quality indicator, the AIS of the GRB are $|AIS_1^{GRB}|=2.9802$ and $|AIS_2^{GRB}|=2.9205$, which are lower than GRU, RBF, and BPNN, indicating that the GRB has excellent interval forecasting performance. In spite of $FINAW_1^{BPNN}=0.0981$,$CWC_1^{BPNN}=0.0981$ and $FINAW_2^{BPNN}=0.1136$,$FINAW_2^{RBF}=0.1131$,$CWC_2^{BPNN}=0.1136$,$CWC_2^{RBF}=0.1131$ are slightly lower than $FINAW_1^{GRB}=0.0983$,$FINAW_2^{GRB}=0.1189$ and $CWC_1^{GRB}=0.0983$,$CWC_1^{GRB}=0.1189$,but other metrics,(i.e., $FICP_1^{GRB}=0.9792$, $FICP_2^{GRB}=0.9875$,$AWD_1^{GRB}=0.0037$, $AWD_2^{GRB}=0.0020$, and $|AIS_1^{GRB}|=2.9205$,$|AIS_1^{GRB}|=2.9802$) are better than the models designed by $FICP_1^{BPNN}=0.9667$, $FICP_2^{RBF}=0.9667$, $FICP_2^{BPNN}=0.9833$, $AWD_1^{BPNN}=0.0075$, $AWD_2^{RBF}=0.0052$, $AWD_2^{BPNN}=0.0025$, and $|AIS_1^{BPNN}|=5.9660$,$|AIS_2^{RBF}|=4.2593$,$|AIS_2^{BPNN}|=3.1824$. The above shows that all indicators must be considered when evaluating a model. The results of both the point and interval forecasts show that the proposed combined crude oil price forecasting model is effective. The error indicator bar charts for points and intervals, as well as the interval forecast results of the developed model, are shown in Fig 2.

B. EXPERIMENT II: COMPARISON OF GRB WITH OTHER MODELS

To demonstrate the superior performance of the developed model, GRB is compared with four other individual models

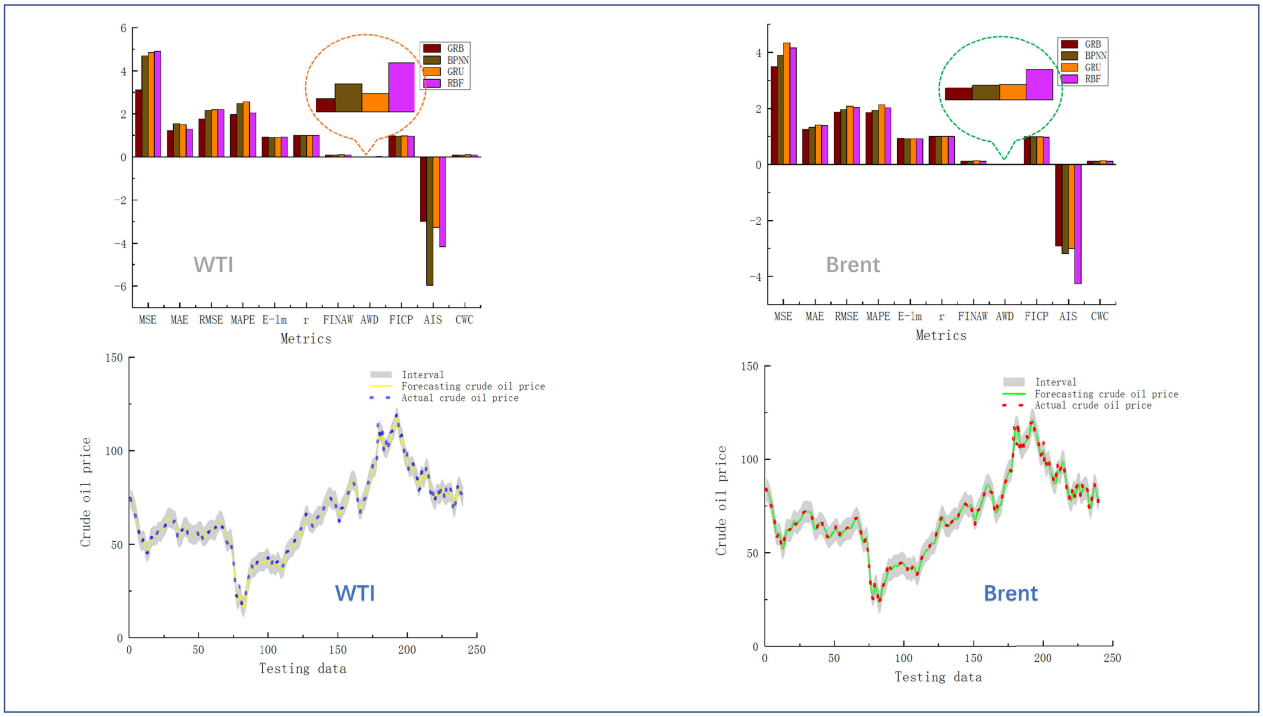

FIGURE 2. Results of experiment I.

TABLE 8. Point forecasting results of experiment I.

Dataset	Metrics	GRU	RBF	BPNN	**GRB**
WTI	MSE	4.8482	4.9038	4.7003	**3.1107**
	MAE	1.5141	1.2946	1.5519	**1.2229**
	RMSE	2.2019	2.2145	2.1680	**1.7637**
	MAPE(%)	2.5681	2.0399	2.4872	**1.9657**
	E-lm	0.9092	0.9224	0.9070	**0.9267**
	r	0.9945	0.9948	0.9964	**0.9964**
Brent	MSE	4.3481	4.1587	3.8882	**3.4824**
	MAE	1.4119	1.3887	1.3266	**1.2571**
	RMSE	2.0852	2.0393	1.9718	**1.8661**
	MAPE(%)	2.1329	2.0284	1.9305	**1.8498**
	E-lm	0.9136	0.9150	0.9188	**0.9230**
	r	0.9951	0.9955	0.9957	**0.9960**

GRB stands for the combined model of GRU, RBF, and BPNN.

TABLE 9. Interval forecasting results of experiment I.

Dataset	Metrics	GRU	RBF	BPNN	**GRB**
WTI	FINAW	0.1115	0.0984	0.0981	**0.0983**
	AWD	0.0050	0.0132	0.0075	**0.0037**
	FICP	0.9792	0.9667	0.9667	**0.9792**
	AIS	-3.2698	-4.1684	-5.9660	**-2.9802**
	CWC	0.1115	0.0984	0.0981	**0.0983**
Brent	FINAW	0.1347	0.1131	0.1136	**0.1189**
	AWD	0.0026	0.0052	0.0025	**0.0020**
	FICP	0.9833	0.9667	0.9833	**0.9875**
	AIS	-3.0021	-4.2593	-3.1824	**-2.9205**
	CWC	0.1347	0.1131	0.1136	**0.1189**

GRB stands for the combined model of GRU, RBF, and BPNN.

(Elman, ELM, biLSTM, RNN). The detailed prediction results are shown in Table 10 - 11, and the visualization of the prediction results is shown in Fig 3 Analysing the point forecasting results for WTI dataset, the values of the individual error metrics of the proposed model are $MSE^{GRB} = 3.1107$, $MAPE^{GRB} = 1.9657\%$,$MAE^{GRB} = 1.2229$, and $RMSE^{GRB} = 1.7637$, $E - lm^{GRB} = 0.9267$,$r^{GRB} = 0.9964$, and the GRB model achieves optimal values for all these metrics. Therefore, the developed model achieved optimal forecasting results compared to the other models. In Brent dataset, the designed model with $MSE^{GRB} = 3.4824$, $MAPE^{GRB} = 1.8498\%$, $MAE^{GRB} = 1.2571$ and $RMSE^{GRB} = 1.8661$, $E - lm^{GRB} = 0.9230$ and $r^{GRB} = 0.9960$ also outperformed the other four models. In summary, the forecasting accuracy of the designed model is the highest.

In the interval forecasting results, it is clear that combined forecasting is important for improving forecasting accuracy. Let us take the results of the WTI dataset as an example. Although $FINAW^{GRB} = 0.0983$ is slightly lower than $FINAW^{Elman} = 0.0952$, the other metrics, $AWD^{GRB} = 0.0037$, $FICP^{GRB} = 0.9792$,$|AIS^{GRB}| = 2.9802$, and $CWC^{GRB} = 0.0983$, are both optimal. For the Brent dataset, the situation is approximately the same. Thus, the validity of the combined model is demonstrated.

C. EXPERIMENT III: VALIDATION OF DATA DENOISING METHODS

To validate the advantages of the ICEEMDAN denoising approach, the other four data denoising methods and no

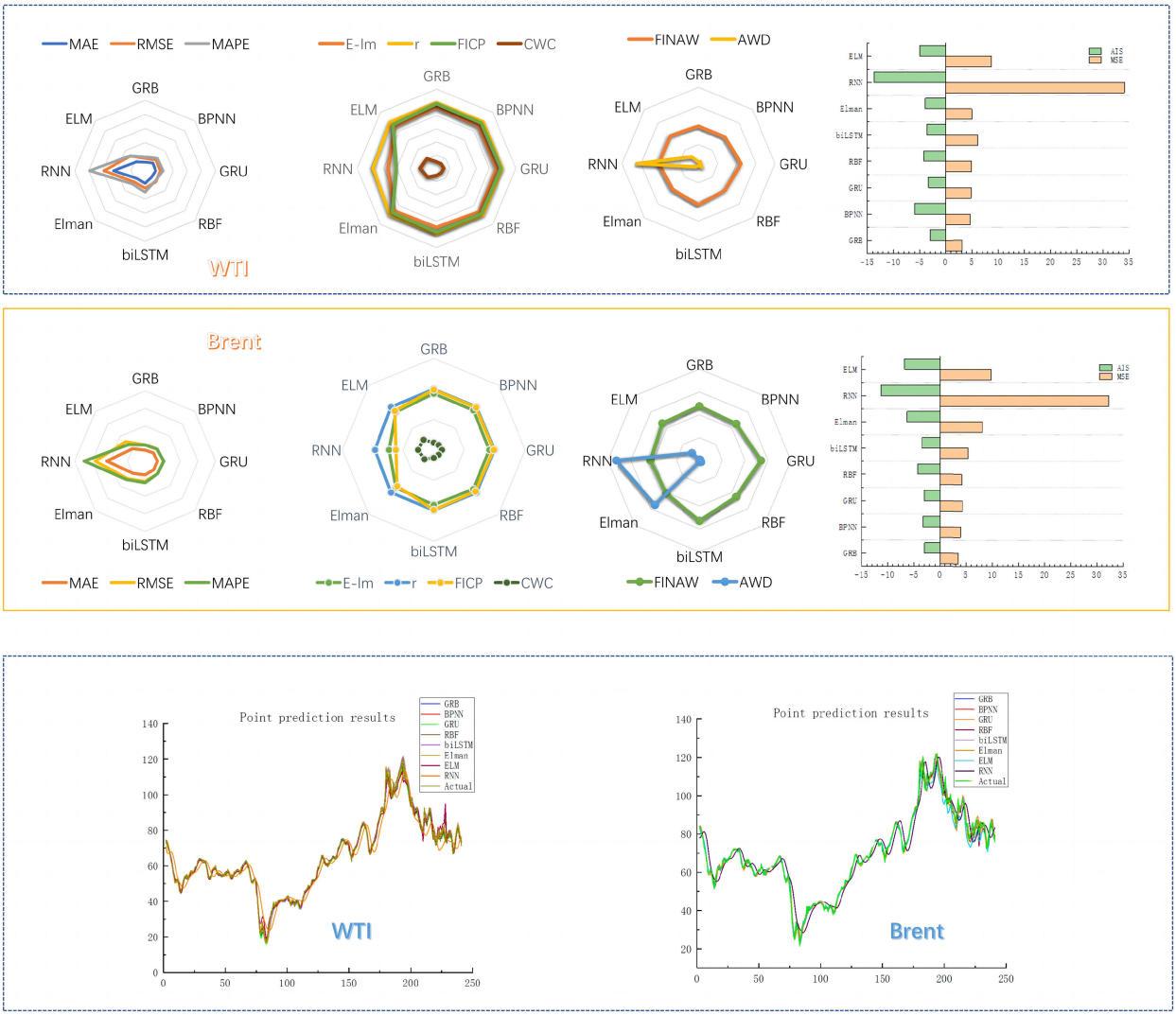

FIGURE 3. Results of experiment II.

TABLE 10. Point forecasting results of experiment II.

Dataset	Metrics	Elman	ELM	biLSTM	RNN	**GRB**
WTI	MSE	4.9670	8.7518	6.0803	34.1754	**3.1107**
	MAE	1.5684	1.7821	1.7774	4.4854	**1.2229**
	RMSE	2.2287	2.9583	2.4658	5.8460	**1.7637**
	MAPE(%)	2.6388	3.0139	3.0274	7.8912	**1.9657**
	E-lm	0.9060	0.8932	0.8935	0.7312	**0.9267**
	r	0.9943	0.9905	0.9941	0.9636	**0.9964**
Brent	MSE	8.0915	9.7870	5.4213	32.3306	**3.4824**
	MAE	1.9739	2.0059	1.5767	4.3590	**1.2571**
	RMSE	2.8446	3.1284	2.3284	5.6860	**1.8661**
	MAPE(%)	2.9870	2.6710	2.4704	6.9207	**1.8498**
	E-lm	0.8792	0.8772	0.9035	0.7332	**0.9230**
	r	0.9911	0.9920	0.9939	0.9625	**0.9960**

GRB stands for the combined model of GRU, RBF, and BPNN.

TABLE 11. Interval forecasting results of experiment II.

Dataset	Metrics	Elman	ELM	biLSTM	RNN	**GRB**
WTI	FINAW	0.0952	0.1031	0.1081	0.1036	**0.0983**
	AWD	0.0117	0.0251	0.0056	0.1619	**0.0037**
	FICP	0.9458	0.9333	0.9667	0.6083	**0.9792**
	AIS	-3.8917	-5.0439	-3.6139	-13.7594	**-2.9802**
	CWC	0.1908	0.2079	0.1081	0.2494	**0.0983**
Brent	FINAW	0.1021	0.1150	0.1323	0.1072	**0.1189**
	AWD	0.1379	0.0230	0.0034	0.1815	**0.0020**
	FICP	0.8458	0.9042	0.9875	0.6208	**0.9875**
	AIS	-6.2685	-6.7353	-3.3984	-11.3665	**-2.9205**
	CWC	0.2153	0.2353	0.1323	0.2561	**0.1189**

GRB stands for the combined model of GRU, RBF, and BPNN.

data denoising are selected for comparison with ICEEMDAN in this experiment. The specific results are summarized in Table 12 - 13, and a visualization of the results is shown in Fig 4.

From the results of the point forecasting experiments, the ICEEMDAN method is optimal compared to other methods of data denoising. Take WTI dataset as an example: $MSE^{ICEEMDAN} = 3.1107$, $MAE^{ICEEMDAN} = 1.2229$, $RMSE^{ICEEMDAN} = 1.7637$, $MAPE^{ICEEMDAN} =$

TABLE 12. Point forecasting results of experiment III.

Dataset	Metrics	No-denoising	VMD	EEMD	CEEMD	CEEMDAN	ICEEMDAN
WTI	MSE	16.6848	6.7200	11.6748	4.9565	7.0824	**3.1107**
	MAE	2.9093	1.8863	2.7513	1.6008	2.0085	**1.2229**
	RMSE	4.0847	2.5923	3.4168	2.2263	2.6613	**1.7637**
	MAPE(%)	4.9712	3.1486	4.0918	2.6931	3.4370	**1.9657**
	E-lm	0.8256	0.8869	0.8316	0.9041	0.8796	**0.9267**
	r	0.9809	0.9924	0.9892	0.9946	0.9920	**0.9964**
Brent	MSE	16.7541	5.9793	4.6930	4.7073	6.4399	**3.4824**
	MAE	2.9228	1.8299	1.5074	1.5520	1.8118	**1.2571**
	RMSE	4.0932	2.4453	2.1663	2.1696	2.5377	**1.8661**
	MAPE(%)	4.5168	2.8238	2.2485	2.3297	2.8591	**1.8498**
	E-lm	0.8211	0.8880	0.9077	0.9050	0.8891	**0.9230**
	r	0.9807	0.9932	0.9948	0.9947	0.9926	**0.9960**

$1.9657\%, E-lm^{ICEEMDAN} = 0.9267, r^{ICEEMDAN} = 0.9964$. These values of the error metric are better than those of the other five data preprocessing methods. In the Brent dataset, the results are also similar. Thus, using an appropriate data denoising method will significantly improve the accuracy of the forecasting model. This conclusion can also be drawn when analyzing the interval forecasting results. Thus, the designed models with values $|AIS^{ICEEMDAN}| = 2.9802$, $FICP^{ICEEMDAN} = 0.9792$ and $AWD^{ICEEMDAN} = 0.0037$ in WTI dataset outperform the other models. This is also true for the results of the Brent dataset. Therefore, the accuracy of the developed model is significantly improved by using an appropriate data preprocessing method.

D. EXPERIMENT IV: COMPARISON OF DIFFERENT MODEL COMBINED METHODS

To test the performance of the MOSSA-based combination approach, four other model combination approaches were selected for comparison: a simple average combination approach By calculating the average forecasting results of the models, the MALO-based combination approach, the MODA-based combination approach, and the MSSA-based combination approach; the simple average combinatorial frame was calculated as shown in (29):

$$P_{final} = \frac{1}{n}\Sigma_{i=1}^{n} P_i, \tag{29}$$

where P_i is the predicted outcome of the ith member model;P_{final} denotes the outcome; n represents the number of member models of the combined model. The specific experimental error results are summarized in Table 14 - 15, and the error visualization is shown in Fig 5. The results show that the MOSSA-based combination method is superior to the other four combinatorial frameworks in point and interval forecasts.

E. EXPERIMENT V: INPUT STRUCTURE WITH MIXED-FREQUENCY DATA VS. NO MIXED-FREQUENCY DATA

The GRB that considers only considers co-frequency variables (i.e., the input variables are structured as $\{x_{t-4}, x_{t-3}, x_{t-2}, x_{t-1}, x_t$, opening price, highest price, lowest price$\}$) is compared with the GRB that considers mixed-frequency variables (i.e., the input variables are structured as $\{x_{t-4}, x_{t-3}, x_{t-2}, x_{t-1}, x_t$, opening price, highest price, lowest price, $USDX_1^t, USDX_2^t, USDX_3^t, USDX_4^t, USDX_5^t\}$). The effectiveness of the confounding variables in improving forecasting accuracy is examined. The specific experimental results are shown in Table 16, and the optimal values of each evaluation index are shown in bold.

In the WTI dataset, considering the mixed-frequency variables, GRB reaches the optimal value for all indicators except $FINAW_{no-mixed-frequency} = 0.980$, which is slightly better than $FINAW_{mixed-frequency} = 0.983$. In Brent dataset, $MAE_{no-mixed-frequency} = 1.2488$, $E-lm_{no-mixed-frequency} = 0.9236$ are slightly better than $MAE_{mixed-frequency} = 1.2571$ and $E-lm_{mixed-frequency} = 0.9230$, but optimal in $MSE_{mixed-frequency} = 3.4824$, $RMSE_{mixed-frequency} = 1.8661$, $MAPE_{mixed-frequency} = 1.8498\%, r_{mixed-frequency} = 0.9960$, $FINAW_{mixed-frequency} = 0.1189$, $AWD_{mixed-frequency} = 0.0020$, $FICP_{mixed-frequency} = 0.9875$, $|AIS_{mixed-frequency}| = 2.9205$. In this way, the validity of the mixed-frequency variables is checked, which helps to improve the accuracy of the forecasts and to bring the forecasting results closer to the actual situation.

VI. DISCUSSION

To further validate the benefits of the proposed model, some discussion is provided in this section.

A. DM TEST

The Diebold-Mariano test [60] is a t-test for the equality of means of a two-loss series of alternative forecasts. The DM test is typically used to determine which model provides the better predictions. The mathematical formula for the DM test is as follows:

$$DM = \frac{\frac{1}{n}\Sigma_{i=1}^{n}\left(e_1^i - e_2^i\right)}{\sqrt{S^2/n}}, \tag{30}$$

where e_1^i and e_2^i are the series of prediction errors for the models being compared; S^2 is the estimate of the standard deviation in $d^i = e_1^i - e_2^i$.

TABLE 13. Interval forecasting results of experiment III.

Dataset	Metrics	No-denoising	VMD	EEMD	CEEMD	CEEMDAN	ICEEMDAN
WTI	FINAW	0.1099	0.1020	0.1082	0.1044	0.1022	**0.0983**
	AWD	0.0383	0.0106	0.0096	0.0076	0.0090	**0.0037**
	FICP	0.8583	0.9458	0.9000	0.9542	0.9417	**0.9792**
	AIS	-6.7801	-4.3318	-7.2500	-3.9290	-4.6635	**-2.9802**
	CWC	0.2303	0.2045	0.2219	0.1044	0.2052	**0.0983**
Brent	FINAW	0.1186	0.1162	0.1286	0.1245	0.1243	**0.1189**
	AWD	0.0296	0.0049	0.0025	0.0024	0.0049	**0.0020**
	FICP	0.8792	0.9667	0.9833	0.9792	0.9708	**0.9875**
	AIS	-7.1995	-4.4204	-3.3105	-4.0621	-4.2839	**-2.9205**
	CWC	0.2460	0.1162	0.1286	0.1245	0.1243	**0.1189**

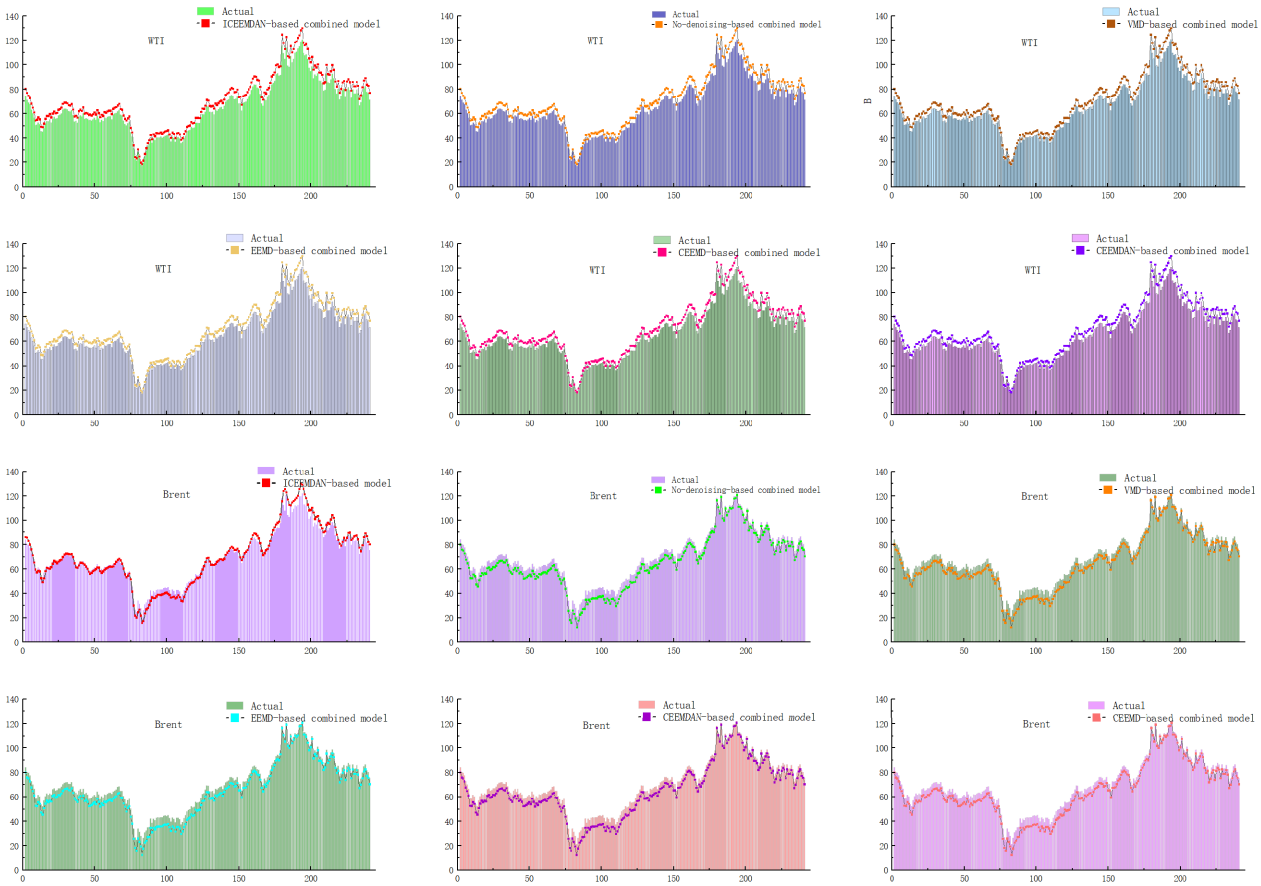

FIGURE 4. The results of experiment III.

The confidence level at which the two models being compared differ significantly in performance can be determined by querying the table of the regular standard distribution for the confidence level corresponding to DM. The experimental results show that all DM test values for the WTI dataset are more significant than $Z_{0.15/2} = 1.44$, and that the designed combined forecasting framework has significantly improved forecasting ability. Moreover, the minimum value of DM in the Brent dataset is 1.8839, more significant than $Z_{0.1/2} = 1.645$, indicating that the designed method outperforms the other methods. More detailed results are given in Table 17.

B. EFFECTIVENESS EVALUATION

Two key indicators, namely first-order forecast effectiveness (FE1) and second-order forecast effectiveness (FE2), are examined to assess the predictive validity [61]. Higher indicator values mean greater validity of the model's predictions.

Table 18 summarizes the test results and highlights the best values in bold. It can be seen from the table that the proposed combined model outperforms the other models in both datasets. Therefore, the proposed combined forecasting model demonstrates superior robustness compared to all other models.

TABLE 14. Point forecasting results of experiment IV.

Dataset	Metrics	Average model	MODA	MSSA	MALO	MOSSA
WTI	MSE	3.8091	3.1364	3.2004	3.8615	**3.1107**
	MAE	1.3229	1.1884	1.1805	1.2758	**1.2229**
	RMSE	1.9517	1.7710	1.7890	1.9651	**1.7637**
	MAPE(%)	2.1173	1.8799	1.8591	2.0979	**1.9657**
	E-lm	0.9207	0.9288	0.9292	0.9235	**0.9267**
	r	0.9961	0.9965	0.9964	0.9956	**0.9964**
Brent	MSE	3.5226	3.7056	3.4741	3.4822	**3.4824**
	MAE	1.2750	1.2957	1.2595	1.2643	**1.2571**
	RMSE	1.8769	1.9250	1.8639	1.8661	**1.8661**
	MAPE(%)	1.8842	1.8898	1.8648	1.8712	**1.8498**
	E-lm	0.9220	0.9207	0.9229	0.9226	**0.9230**
	r	0.9960	0.9958	0.9960	0.9960	**0.9960**

GRB stands for the combined model of GRU, RBF, and BPNN.

TABLE 15. Interval forecasting results of experiment IV.

Dataset	Metrics	Average model	MODA	MSSA	MALO	MOSSA
WTI	FINAW	0.1031	0.0983	0.0983	0.1047	**0.0983**
	AWD	0.0059	0.0044	0.0050	0.0064	**0.0037**
	FICP	0.9667	0.9708	0.9708	0.9708	**0.9792**
	AIS	-4.2501	-3.1775	-3.1659	-3.1789	**-2.9802**
	CWC	0.1031	0.0983	0.0983	0.1047	**0.0983**
Brent	FINAW	0.1213	0.1184	0.1200	0.1197	**0.1189**
	AWD	0.0022	0.0021	0.0023	0.0024	**0.0020**
	FICP	0.9833	0.9875	0.9833	0.9833	**0.9875**
	AIS	-3.3598	-3.0277	-3.0767	-3.1678	**-2.9205**
	CWC	0.1213	0.1184	0.1200	0.1197	**0.1189**

GRB stands for the combined model of GRU, RBF, and BPNN.

TABLE 16. Results of experiment V.

Dataset	Metrics	No-mixed-frequeny	Mixed-frequeny
WTI	MSE	3.2668	**3.1107**
	MAE	1.2512	**1.2229**
	RMSE	1.8074	**1.7637**
	MAPE(%)	2.1035	**1.9657**
	E-lm	0.9250	**0.9267**
	r	0.9963	**0.9964**
Brent	FINAW	**0.0980**	0.0983
	AWD	0.0041	**0.0037**
	FICP	0.9792	**0.9792**
	AIS	-3.2116	**-2.9802**
	MSE	3.5956	**3.4824**
	MAE	**1.2488**	1.2571
	RMSE	1.8962	**1.8661**
	MAPE(%)	1.8731	**1.8498**
	E-lm	**0.9236**	0.9230
	r	0.9960	**0.9960**
	FINAW	0.1202	**0.1189**
	AWD	0.0034	**0.0020**
	FICP	0.9875	**0.9875**
	AIS	-2.9218	**-2.9205**

TABLE 17. DM test results.

Model	WTI	Brent
BPNN	4.4129*	1.8879•
GRU	3.5737*	3.0322*
RBF	1.5011*	1.9019•
Elman	4.0282*	5.6724*
ELM	2.5827*	4.8896*
RNN	8.1838*	7.9792*
biLSTM	4.6740*	5.2612*
No-denoising-based combined model	5.4281*	6.2093*
VMD-based model	4.1684*	2.9831*
EEMD-based combined model	8.5616*	3.4528*
CEEMD-based combined model	3.7643*	3.6070*
CEEMDAN-based combined model	6.9063*	5.9654*

$*$ Is the 0.01 significance interval
• Is the 0.1 significance interval
$\star$ Is the 0.15 significance interval

TABLE 18. The forecasting effectiveness of models.

Model	WTI		Brent	
	FE1	FE2	FE1	FE2
BPNN	0.9667	0.7931	0.9833	0.8574
GRU	0.9792	0.8393	0.9833	0.8574
RBF	0.9667	0.7931	0.9667	0.7931
Elman	0.9458	0.7317	0.8458	0.5404
ELM	0.9333	0.7005	0.9042	0.638
RNN	0.6083	0.3114	0.6208	0.3196
biLSTM	0.9667	0.7931	0.9875	0.8778
No-denoising-based combined model	0.8583	0.5590	0.8792	0. 5926
VMD-based combined model	0.9458	0.7317	0.9667	0.7931
EEMD-based combined model	0.9000	0.6300	0.9833	0.8574
CEEMD-based combined model	0.9542	0.7546	0.9792	0.8393
CEEMDAN-based combined model	0.9417	0.7210	0.9708	0.8075
Proposed model	**0.9792**	**0.8393**	**0.9875**	**0.8778**

TABLE 19. Model stability.

Model	WTI	Brent
BPNN	2.3016	2.1371
GRU	2.5664	2.3645
RBF	3.2413	2.2396
Elman	2.5178	4.2127
ELM	5.5991	5.7876
RNN	14.1159	13.3855
biLSTM	2.9334	2.9477
No-denoising-based combined model	8.2552	8.2456
VMD-based combined model	3.1750	2.6416
EEMD-based combined model	4.1221	2.4308
CEEMD-based combined model	2.4039	2.3083
CEEMDAN-based combine dmodel	3.0612	3.1704
Proposed model	**1.6220**	**1.9100**

C. STABILITY ANALYSIS

The variance is a measure of how discrete a data set is. The higher the variance for the same sample, the more volatile the data. Therefore, the variance of the prediction error is introduced to verify the stability of the proposed model. The detailed results are presented in Table 19, where the bold values indicate the best results. The stability results for the evolved models in the two data sets were 1.6220 and 1.9100, respectively, which is the best of all results and means that the evolved models have the most robust stability. The comparison of the models shows that the forecasting values of the combined models are consistently smaller than those of the individual models, indicating that applying the combined framework can improve the stability of the predictions. In addition, the combined models were compared with different data preprocessing techniques, and the ICEEMDAN model produced the best stability results in both data sets. The

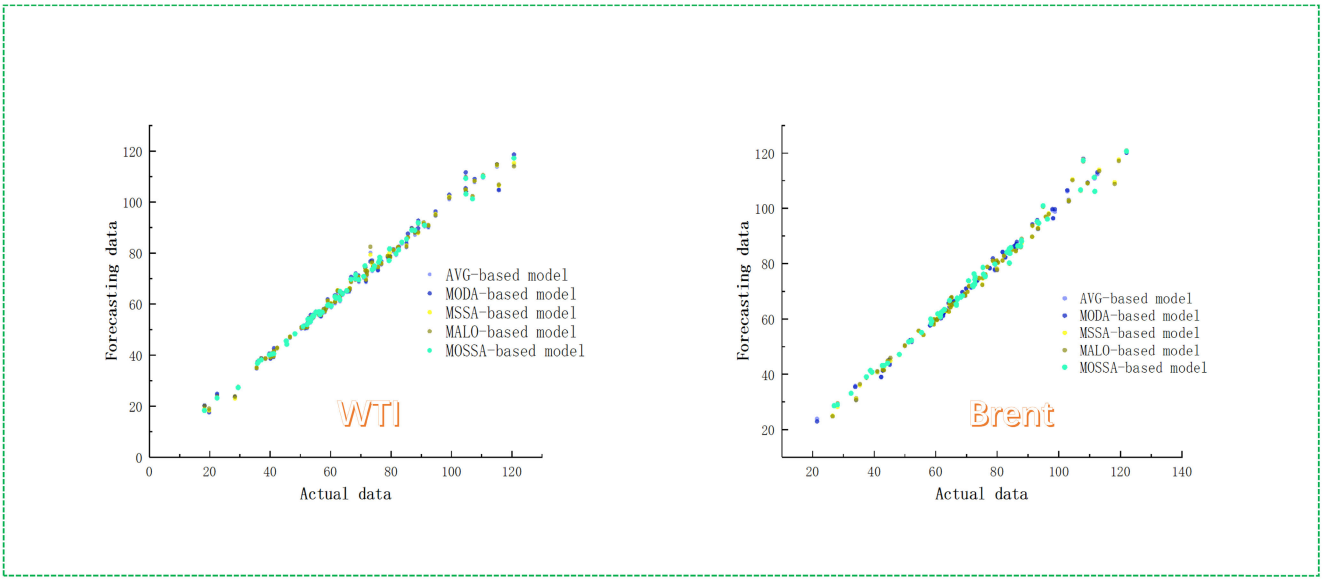

FIGURE 5. The results of experiment IV.

TABLE 20. The effect of the order of crude oil price history variables on the model.

Dataset	Dimension	MSE	MAE	RMSE	MAPE	E-lm	r	FINAW	AWD	FICP	AIS
WTI	1	4.8625	1.5450	2.2051	2.6309	0.9074	0.9948	0.1095	0.0056	0.9708	-2.8672
	2	5.2241	1.5382	2.2856	2.5741	0.9078	0.9941	0.1033	0.0084	0.9708	-3.7337
	3	3.9166	1.3548	1.9790	2.2288	0.9188	0.9956	0.0997	0.0054	0.9833	-3.5567
	4	3.6653	1.3958	1.9145	2.2648	0.9163	0.9961	0.0999	0.0045	0.9875	-4.2817
	5	**3.0277**	**1.2051**	**1.7400**	**1.9456**	**0.9278**	**0.9966**	**0.0994**	0.0032	0.9833	**-2.8368**
	6	3.1787	1.2377	1.7829	1.9815	0.9258	0.9964	0.1013	0.0035	0.9792	-3.0324
	7	3.2403	1.2889	1.8001	2.0788	0.9227	0.9964	0.1000	**0.0031**	**0.9875**	-2.9439
	8	3.5438	1.3107	1.8825	2.1202	0.9214	0.9960	0.1035	0.0038	0.9833	-3.0574
Brent	1	4.9458	1.5105	2.2239	2.2946	0.9075	0.9945	0.1272	0.0036	0.9833	-3.0921
	2	4.8727	1.4908	2.2074	2.2476	0.9087	0.9944	0.1241	0.0038	0.9792	-3.6270
	3	4.0027	1.3425	2.0007	2.0047	0.9178	0.9954	0.1166	0.0048	0.9833	-3.1779
	4	3.5621	1.2935	1.8873	1.8789	0.9208	0.9959	0.1185	0.0026	0.9833	-3.0561
	5	**2.9049**	**1.1406**	**1.7044**	**1.6693**	**0.9302**	**0.9967**	**0.1144**	**0.0024**	**0.9833**	**-2.7409**
	6	3.7158	1.2961	1.9276	1.9444	0.9207	0.9959	0.1202	0.0032	0.9833	-2.7431
	7	3.4072	1.2786	1.8459	1.9027	0.9217	0.9961	0.1209	0.0023	0.9875	-3.0089
	8	3.5676	1.3260	1.8888	1.9520	0.9188	0.9959	0.1200	0.0024	0.9875	-3.3327

TABLE 21. Comparison results.

Dataset	Model	MAPE(%)	MAE	RMSE	r	FINAW	FICP	CWC
Brent	**GRB**	**1.8498**	**1.2571**	**1.8661**	**0.9960**	**0.1189**	**0.9875**	**0.1189**
	Wu's model	5.0178	2.133	3.0802	0.9756	0.2277	0.9718	0.2277
WTI	**GRB**	**1.9657**	**1.2229**	**1.7637**	-	-	-	-
	Zhang's model	1.84	2.48	2.99	-	-	-	-
	Wang's model	2.21	1.49	1.88	-	-	-	-
	Xu's model	5.43	1.93	2.74	-	-	-	-

GRB stands for the model designed for this study.

stability of the model was improved after denoising with the ICEEMDAN data preprocessing technique.

D. SENSITIVITY ANALYSIS

To determine the optimal order of the effect of the crude oil price historical variable on the model, This paper discusses the selection of its historical variables. To validate the impact of the crude oil price history variable on the model, this paper compares experiments where the order of the crude oil price history variable is between 1 and 8. Table 20 shows the specific experimental results, which indicate that in both datasets, each valuation index is optimized when the order of the historical variables is 5. Assuming that x_{t+1} is the output variable at time t+1, $\{x_{t-4}, x_{t-3}, x_{t-2}, x_{t-1}, x_t\}$ are identified

as the input variables for the crude oil price history for both datasets.

E. COMPARATIVE EXAMINATION

The above experimental results demonstrate the effectiveness of the proposed model. However, conclusions based solely on experimental mechanisms may need more convincing. For a fair comparison, this section compares and analyzes the model with other similar studies. We selected Zhang model [6], Wang model [62], Xu model [63], and Wu model [64] for comparison. Zhang et al. used data preprocessing, least squares support vector machine, and particle swarm optimization (LSSVM PSO) methods, as well as a generalized autoregressive conditional heteroscedasticity (GARCH) hybrid model to predict crude oil prices, achieving high prediction accuracy. Xu et al. proposed R-EEMD-RVFL and R-VMD-RVFL models based on Random Vector Function Chain (RVFL) neural networks. Wang et al. proposed a semi-heterogeneous mixed crude oil method for oil price prediction, which combines a set of decomposition methods and a set of interaction prediction techniques. However, the models of Zhang, Wang, and Xu et al. overlooked the importance of uncertainty prediction and did not conduct relevant research on uncertainty prediction. Wu et al. used the Hampel identifier to remove outliers from the crude oil price sequence and then used a complete ensemble empirical mode decomposition to reduce noise. They proposed an improved multi-objective water circulation algorithm to optimize the parameters of the echo state network. Finally, deterministic and uncertain predictions were conducted to validate the model, but there needed to be more exploration of mixed data. Table 21 shows the comparison results between this study and other studies.

VII. CONCLUSION

The fluctuation of crude oil prices has a significant impact on global economic, market, and geopolitical stability. Accurately forecasting crude oil prices can help all parties better respond to market changes, reduce risks, optimize resource allocation, and improve competitiveness. To overcome the limitations of crude oil forecasting models that consider only a single variable or only co-frequency variables, this paper proposes a new multivariate combined mixed-frequency forecasting framework for predicting weekly closing prices of crude oil futures. The framework considers several co-frequency variables and one high-frequency variable simultaneously to improve the forecasting performance. In addition, an advanced data denoising technique is introduced to reduce the interference from data noise, a practical feature selection module is introduced to select appropriate variables to reduce model redundancy, and a multiobjective sparrow search algorithm is used to combine a single model to obtain a more accurate and stable combined forecasting model. Finally, the desired prediction results are obtained.

To verify the superior performance of the proposed model, two data sets, WTI crude oil, and Brent crude oil, were selected for an empirical study, six indexes were selected to evaluate the point forecasting performance, and five indexes were selected to evaluate the interval forecasting. The forecasting results show that the designed forecasting model outperforms other benchmark models with which the model is compared; specifically, the values of MSE are 3.1-3.5, MAE is 1.22-1.25, the accuracy of MAPE is 1.8%-1.9%, the value of FINAW is 0.09-0.12. The interval coverage ratio (FICP) is over 95%. All these metric values are better than those of other models. Therefore, the proposed crude oil forecasting model can be used as an effective technique to predict crude oil prices.

The combination model developed in this article achieves superior point forecasting and interval forecasting performance in weekly crude oil price forecasting. In summary, accurate crude oil price predictions are significant to various stakeholders as they can help them better respond to market changes, mitigate risks, optimize decision-making, and promote sustainable development. In addition, it can also be applied to neighborhoods such as stock markets, finance, and meteorology. Of course, there are still some limitations in this study. Firstly, we did not consider some potential influencing factors, such as supply and demand, political factors, exchange rate fluctuations, etc., which may have a significant impact on crude oil prices. Secondly, this study only predicted weekly crude oil prices without considering long-term crude oil price predictions. Therefore, more research is needed in the future to comprehensively explore the fluctuations and trends of crude oil prices to understand market dynamics better.

REFERENCES

[1] Y. Fang, W. Wang, P. Wu, and Y. Zhao, "A sentiment-enhanced hybrid model for crude oil price forecasting," *Expert Syst. Appl.*, vol. 215, Apr. 2023, Art. no. 119329.

[2] J. Yuan, J. Li, and J. Hao, "A dynamic clustering ensemble learning approach for crude oil price forecasting," *Eng. Appl. Artif. Intell.*, vol. 123, Aug. 2023, Art. no. 106408.

[3] Y. Wang and X. Hao, "Forecasting the real prices of crude oil: What is the role of parameter instability?" *Energy Econ.*, vol. 117, Jan. 2023, Art. no. 106483.

[4] J. Wang, H. Zhou, T. Hong, X. Li, and S. Wang, "A multi-granularity heterogeneous combination approach to crude oil price forecasting," *Energy Econ.*, vol. 91, Sep. 2020, Art. no. 104790.

[5] J. Li, L. Tang, and S. Wang, "Forecasting crude oil price with multilingual search engine data," *Phys. A, Stat. Mech. Appl.*, vol. 551, Aug. 2020, Art. no. 124178.

[6] J.-L. Zhang, Y.-J. Zhang, and L. Zhang, "A novel hybrid method for crude oil price forecasting," *Energy Econ.*, vol. 49, pp. 649–659, May 2015.

[7] S. Sun, Y. Sun, S. Wang, and Y. Wei, "Interval decomposition ensemble approach for crude oil price forecasting," *Energy Econ.*, vol. 76, pp. 274–287, Oct. 2018.

[8] Y.-X. Wu, Q.-B. Wu, and J.-Q. Zhu, "Improved EEMD-based crude oil price forecasting using LSTM networks," *Phys. A, Stat. Mech. Appl.*, vol. 516, pp. 114–124, Feb. 2019.

[9] P. Debaeke, F. Attia, L. Champolivier, J.-F. Dejoux, A. Micheneau, A. A. Bitar, and R. Trépos, "Forecasting sunflower grain yield using remote sensing data and statistical models," *Eur. J. Agronomy*, vol. 142, Jan. 2023, Art. no. 126677.

[10] M. Heidarpanah, F. Hooshyaripor, and M. Fazeli, "Daily electricity price forecasting using artificial intelligence models in the Iranian electricity market," *Energy*, vol. 263, Jan. 2023, Art. no. 126011.

[11] T. Niu, J. Wang, H. Lu, W. Yang, and P. Du, "A learning system integrating temporal convolution and deep learning for predictive modeling of crude oil price," *IEEE Trans. Ind. Informat.*, vol. 17, no. 7, pp. 4602–4612, Jul. 2021.

[12] Y. Gao, J. Wang, and H. Yang, "A multi-component hybrid system based on predictability recognition and modified multi-objective optimization for ultra-short-term onshore wind speed forecasting," *Renew. Energy*, vol. 188, pp. 384–401, Apr. 2022.

[13] V. Shahbazbegian, H. Hosseininesaz, M. Shafie-Khah, and M. Elmusrati, "Forecasting crude oil prices using a hybrid model combining long short-term memory neural networks and Markov switching model," in *Proc. Int. Conf. Future Energy Solutions (FES)*, Vaasa, Finland, Jun. 2023, pp. 1–6.

[14] N. Xu, Z. Wang, Y. Dai, Q. Li, W. Zhu, R. Wang, and R. B. Finkelman, "Prediction of higher heating value of coal based on gradient boosting regression tree model," *Int. J. Coal Geol.*, vol. 274, Jun. 2023, Art. no. 104293.

[15] J. Liu, C. Cheng, C. Zheng, X. Wang, and L. Wang, "Rutting prediction using deep learning for time series modeling and K-means clustering based on RIOHTrack data," *Construction Building Mater.*, vol. 385, Jul. 2023, Art. no. 131515.

[16] Z. Tan, J. Zhang, J. Wang, and J. Xu, "Day-ahead electricity price forecasting using wavelet transform combined with ARIMA and GARCH models," *Appl. Energy*, vol. 87, no. 11, pp. 3606–3610, Nov. 2010.

[17] S. Alexiadis, "Forecasting agricultural production using co-integration analysis," *Land Use Policy*, vol. 61, pp. 466–474, Feb. 2017.

[18] H. Mohammadi and L. Su, "International evidence on crude oil price dynamics: Applications of ARIMA-GARCH models," *Energy Econ.*, vol. 32, no. 5, pp. 1001–1008, Sep. 2010.

[19] J. Guo, C.-X. Gu, J.-J. Yang, Y. Zhang, and H. Yang, "Data mining and application of ship impact spectrum acceleration based on PNN neural network," *Ocean Eng.*, vol. 203, May 2020, Art. no. 107193.

[20] C. Zhu, X. Ma, C. Zhang, W. Ding, and J. Zhan, "Information granules-based long-term forecasting of time series via BPNN under three-way decision framework," *Inf. Sci.*, vol. 634, pp. 696–715, Jul. 2023.

[21] G. Sideratos and N. D. Hatziargyriou, "A distributed memory RBF-based model for variable generation forecasting," *Int. J. Electr. Power Energy Syst.*, vol. 120, Sep. 2020, Art. no. 106041.

[22] S. Zhang, J. Luo, S. Wang, and F. Liu, "Oil price forecasting: A hybrid GRU neural network based on decomposition–reconstruction methods," *Expert Syst. Appl.*, vol. 218, May 2023, Art. no. 119617.

[23] I. Kumar, B. K. Tripathi, and A. Singh, "Attention-based LSTM network-assisted time series forecasting models for petroleum production," *Eng. Appl. Artif. Intell.*, vol. 123, Aug. 2023, Art. no. 106440.

[24] S. N. Singh and A. Mohapatra, "Data driven day-ahead electrical load forecasting through repeated wavelet transform assisted SVM model," *Appl. Soft Comput.*, vol. 111, Nov. 2021, Art. no. 107730.

[25] R. Prasad, M. Ali, P. Kwan, and H. Khan, "Designing a multi-stage multivariate empirical mode decomposition coupled with ant colony optimization and random forest model to forecast monthly solar radiation," *Appl. Energy*, vol. 236, pp. 778–792, Feb. 2019.

[26] T. Yin and Y. Wang, "Predicting the price of WTI crude oil futures using artificial intelligence model with chaos," *Fuel*, vol. 316, May 2022, Art. no. 122523.

[27] X. Liang, P. Luo, X. Li, X. Wang, and L. Shu, "Crude oil price prediction using deep reinforcement learning," *Resour. Policy*, vol. 81, Mar. 2023, Art. no. 103363.

[28] J. Wang, H. Zhang, Q. Li, and A. Ji, "Design and research of hybrid forecasting system for wind speed point forecasting and fuzzy interval forecasting," *Expert Syst. Appl.*, vol. 209, Dec. 2022, Art. no. 118384.

[29] G. Li, S. Yin, and H. Yang, "A novel crude oil prices forecasting model based on secondary decomposition," *Energy*, vol. 257, Jan. 2022, Art. no. 124684.

[30] P. Jiang, Y. Nie, J. Wang, and X. Huang, "Multivariable short-term electricity price forecasting using artificial intelligence and multi-input multi-output scheme," *Energy Econ.*, vol. 117, Jan. 2023, Art. no. 106471.

[31] J. Wang, Y. Wang, Z. Li, H. Li, and H. Yang, "Design of a combined system based on multi-objective optimization for point and interval forecasting of air pollution," *Expert Syst. Appl.*, vol. 191, Apr. 2022, Art. no. 116345.

[32] P. Jiang, Z. Liu, J. Wang, and L. Zhang, "Decomposition-selection-ensemble forecasting system for energy futures price forecasting based on multi-objective version of chaos game optimization algorithm," *Resour. Policy*, vol. 73, Oct. 2021, Art. no. 102234.

[33] J. Zhang and N. Tansu, "Optical gain and laser characteristics of InGaN quantum wells on ternary InGaN substrates," *IEEE Photon. J.*, vol. 5, no. 2, Apr. 2013, Art. no. 2600111.

[34] X.-A. Ma, H. Xu, and C. Ju, "Class-specific feature selection via maximal dynamic correlation change and minimal redundancy," *Expert Syst. Appl.*, vol. 229, Nov. 2023, Art. no. 120455.

[35] J. Bai, J. Guo, B. Sun, Y. Guo, Q. Bao, and X. Xiao, "Intelligent forecasting model of stock price using neighborhood rough set and multivariate empirical mode decomposition," *Eng. Appl. Artif. Intell.*, vol. 122, Jun. 2023, Art. no. 106106.

[36] I. Guyon and A. Elisseeff, "An introduction to variable and feature selection," *J. Mach. Learn. Res.*, vol. 3, pp. 1157–1182, Jan. 2003.

[37] Z. Shao, S. Yang, F. Gao, K. Zhou, and P. Lin, "A new electricity price prediction strategy using mutual information-based SVM-RFE classification," *Renew. Sustain. Energy Rev.*, vol. 70, pp. 330–341, Apr. 2017.

[38] H. Peng, F. Long, and C. Ding, "Feature selection based on mutual information criteria of max-dependency, max-relevance, and min-redundancy," *IEEE Trans. Pattern Anal. Mach. Intell.*, vol. 27, no. 8, pp. 1226–1238, Aug. 2005.

[39] J. Wang, Y. Zhou, and H. Jiang, "A novel interval forecasting system based on multi-objective optimization and hybrid data reconstruct strategy," *Expert Syst. Appl.*, vol. 217, May 2023, Art. no. 119539.

[40] S. Urolagin, N. Sharma, and T. K. Datta, "A combined architecture of multivariate LSTM with Mahalanobis and Z-score transformations for oil price forecasting," *Energy*, vol. 231, Sep. 2021, Art. no. 120963.

[41] E. Ghysels and R. Valkanov, "The MIDAS touch: Mixed data sampling regression models," *CiranoWork. Papers*, vol. 5, no. 1, pp. 512–517, 2004.

[42] L. Ding, Z. Zhao, and L. Wang, "Probability density forecasts for natural gas demand in China: Do mixed-frequency dynamic factors matter?" *Appl. Energy*, vol. 312, Apr. 2022, Art. no. 118756.

[43] Y.-Y. Zhang and Y.-J. Zhang, "The impact of institutional analyst forecast divergence on crude oil market: Evidence from the mixed frequency models," *Int. Rev. Financial Anal.*, vol. 84, Nov. 2022, Art. no. 102418.

[44] Y.-J. Zhang and J.-L. Wang, "Do high-frequency stock market data help forecast crude oil prices? Evidence from the MIDAS models," *Energy Econ.*, vol. 78, pp. 192–201, Feb. 2019.

[45] Y. Hao, W. Yang, and K. Yin, "Novel wind speed forecasting model based on a deep learning combined strategy in urban energy systems," *Expert Syst. Appl.*, vol. 219, Jun. 2023, Art. no. 119636.

[46] S. Degiannakis and G. Filis, "Forecasting oil prices: High-frequency financial data are indeed useful," *Energy Econ.*, vol. 76, pp. 388–402, Oct. 2018.

[47] J. Wang, X. Niu, L. Zhang, and M. Lv, "Point and interval prediction for non-ferrous metals based on a hybrid prediction framework," *Resour. Policy*, vol. 73, Oct. 2021, Art. no. 102222.

[48] J. Wang, Y. Wang, H. Li, H. Yang, and Z. Li, "Ensemble forecasting system based on decomposition-selection-optimization for point and interval carbon price prediction," *Appl. Math. Model.*, vol. 113, pp. 262–286, Jan. 2023.

[49] M. A. Colominas, G. Schlotthauer, and M. E. Torres, "Improved complete ensemble EMD: A suitable tool for biomedical signal processing," *Biomed. Signal Process. Control*, vol. 14, pp. 19–29, Nov. 2014.

[50] C. Yuan, Z. Hu, Y. Liu, S. He, and J. Du, "Application of ICEEMDAN to noise reduction of near-seafloor geomagnetic field survey data," *J. Appl. Geophysics*, vol. 209, Feb. 2023, Art. no. 104933.

[51] Y. Liang, Y. Lin, and Q. Lu, "Forecasting gold price using a novel hybrid model with ICEEMDAN and LSTM-CNN-CBAM," *Expert Syst. Appl.*, vol. 206, Nov. 2022, Art. no. 117847.

[52] C. Emeksiz and M. Tan, "Wind speed estimation using novelty hybrid adaptive estimation model based on decomposition and deep learning methods (ICEEMDAN-CNN)," *Energy*, vol. 249, Jun. 2022, Art. no. 123785.

[53] J. Sun, P. Zhao, and S. Sun, "A new secondary decomposition-reconstruction-ensemble approach for crude oil price forecasting," *Resour. Policy*, vol. 77, Aug. 2022, Art. no. 102762.

[54] M. Lee, J.-H. Lee, and D.-H. Kim, "Gender recognition using optimal gait feature based on recursive feature elimination in normal walking," *Expert Syst. Appl.*, vol. 189, Mar. 2022, Art. no. 116040.

[55] T. Deng, Y. Huang, G. Yang, and C. Wang, "Pointwise mutual information sparsely embedded feature selection," *Int. J. Approx. Reasoning*, vol. 151, pp. 251–270, Dec. 2022.

[56] Y. Dai, J. Guo, L. Yang, and W. You, "A new approach of intelligent physical health evaluation based on GRNN and BPNN by using a wearable smart bracelet system," *Proc. Comput. Sci.*, vol. 147, pp. 519–527, Jan. 2019.
[57] G. Li, S. Chen, S. Jia, Z. Lu, J. Cai, S. Jiang, Y. Cao, P. Sun, H. Xu, J. Fan, J. Li, and S. Jing, "Prediction of explosives by a de-broadening model based on RBF neural network," *Nucl. Instrum. Methods Phys. Res. A, Accel. Spectrom. Detect. Assoc. Equip.*, vol. 1057, Dec. 2023, Art. no. 168780.
[58] R. B. T. Cahuantzi, X. Y. Chen, and S. F. Güttel, "A comparison of LSTM and GRU networks for learning symbolic sequences," in *Proc. Sci. Inf. Conf.*, 2023, pp. 771–785.
[59] J. Xue and B. Shen, "A novel swarm intelligence optimization approach: Sparrow search algorithm," *Syst. Sci. Control Eng.*, vol. 8, no. 1, pp. 22–34, Jan. 2020.
[60] F. X. Diebold and R. S. Mariano, "Comparing predictive accuracy," *J. Bus. Econ. Statist.*, vol. 13, no. 3, p. 253, Jul. 1995.
[61] W. Yang, J. Wang, H. Lu, T. Niu, and P. Du, "Hybrid wind energy forecasting and analysis system based on divide and conquer scheme: A case study in China," *J. Cleaner Prod.*, vol. 222, pp. 942–959, Jun. 2019.
[62] J. Wang, X. Li, T. Hong, and S. Wang, "A semi-heterogeneous approach to combining crude oil price forecasts," *Inf. Sci.*, vols. 460–461, pp. 279–292, Sep. 2018.
[63] K. Xu and H. Niu, "Denoising or distortion: Does decomposition-reconstruction modeling paradigm provide a reliable prediction for crude oil price time series?" *Energy Econ.*, vol. 128, Dec. 2023, Art. no. 107129.
[64] C. Wu, J. Wang, and Y. Hao, "Deterministic and uncertainty crude oil price forecasting based on outlier detection and modified multi-objective optimization algorithm," *Resour. Policy*, vol. 77, Aug. 2022, Art. no. 102780.

JUN LONG received the Bachelor of Science degree in mathematics and applied mathematics from Beibu Gulf University, Qinzhou, China, in 2021. He is currently pursuing the master's degree in mathematics with the School of Mathematics and Information Science, Guangxi University. His research interests include big data and artificial intelligence theory and algorithms, optimization theory and methods, and applied mathematics.

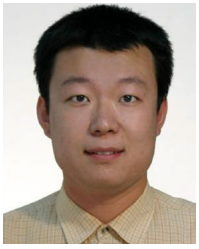

LUE LI received the Ph.D. degree in management science and engineering from Chongqing University, Chongqing, China, in 2019. He is currently a Lecturer with the Guangxi Key Laboratory of Cross-Border E-Commerce Intelligent Information Processing, School of Information and Statistics, Guangxi University of Finance and Economics. His research interests include artificial intelligence and their application in prediction of clean energies.

ZEJUN LI received the Bachelor of Science degree in applied physics from Sichuan Agricultural University, China, in 2020. He is currently pursuing the master's degree in mathematics with the School of Mathematics and Information Science, Guangxi University. His research interests include big data and artificial intelligence theory and algorithms, optimization theory and methods, and applied mathematics.